Not so simple "simply-folded Zagros": the role of pre-collisional extensional faulting, salt tectonics and multi-stage thrusting in the Sarvestan transfer zone (Fars, Iran)

Eugenio Carminati[1], Luca Aldega[1], Sabina Bigi[1], Giorgio Minelli[2], Ali Shaban[3]

1) Dipartimento di Scienze della Terra, Sapienza Università di Roma, Rome, Italy
2) Dipartimento di Fisica e Geologia, Università degli Studi di Perugia, Perugia, Italy
3) National Iranian Oil Company, Tehran, Iran

The corresponding author is:
Eugenio Carminati
Dipartimento di Scienze della Terra
Universita' degli Studi di Roma "La Sapienza"
P.le Aldo Moro 5
I-00185 Roma Italia
Tel.: +39-06-49914950
Fax: +39-06-4454729
e-mail: eugenio.carminati@uniroma1.it

Abstract

The Sarvestan plain is bounded by highly elevated anticlines associated with thrusts or transpressional faults and hosts the NNW-SSE Sarvestan transfer zone. Surface and subsurface geological data, and 22 seismic lines allowed us to reconstruct the 3D geometry of the area. Mixed layers illite-smectite and 1D burial and thermal modelling were used to constrain the complex geological evolution of the Sarvestan plain where inherited structures strongly controlled the geometry of syn-to post-collisional contractional structures. Paleozoic-Mesozoic rifting related extension generated E-W and NNW-SSE normal fault systems. Such faults were associated with changes in the thickness of the sedimentary cover. Lateral facies changes were later induced by the Cretaceous obduction of ophiolites, cropping out some tens of km north of the study area. During the Miocene the footwall and the hanging wall of the Sarvestan fault had different thermal evolution. This is tentatively explained by flow of Cambrian salt from the plain area towards the hanging wall of the Sarvestan fault, associated with salt diapirism during Lower-Middle Miocene time. Salt tectonics is invoked also to explain, at least in part, the development of the overturned anticline in the hanging wall of the Sarvestan fault. An early phase of contractional deformation occurred in the Middle Miocene (since 15 My, i.e., after the deposition of the Agha Jari Fm) generating the E-W oriented folds buried below the plain, likely inverting inherited normal faults. The erosion of these structures was followed by the deposition of the Bakhtiari Fm conglomerates in Middle-Late Miocene times. A later phase of contractional tectonics generated the thrust faults and the anticlines bounding the Sarvestan plain some 6-5 My ago. The Sarvestan dextral transpressional fault, that likely acted as a strongly oblique ramp of the Maharlu thrust, mainly structured in this period, although its activity may have continued until present.

Keywords: Zagros; salt tectonics; thrusting; transfer zone; Sarvestan

1. Introduction

The geometry of contractional structures in the Zagros fold-and-thrust belt (Fig. 1) was influenced by facies and thickness changes in the stratigraphy (e.g., James and Wynd, 1965; Alavi, 2004). Such changes were induced mainly by Paleozoic to Mesozoic thick-skinned extensional tectonics and by shallow-rooted Tertiary extensional faults (Navabpour et al., 2010).

The most important stratigraphic change occurs between the Dezful Embayment and the Fars region, respectively characterized by the absence and presence of Cambrian evaporites (Hormuz Fm) at the bottom of the deformed succession. The front of the belt is characterized by a salient (i.e., by larger advancement of the compressional front) in the Fars region (Fig. 1), and a recess in the Dezful Embayment, (Allen and Talebian, 2011), as predicted by sand-box models. Cambrian salt also controls strain distribution in the belt (Carminati et al., 2013). The larger advancement of the thrust fronts in the SE part (Fig. 1) is accommodated by a major N-S transfer zone (Kazerun fault; Sepehr and Cosgrove, 2005; Carminati et al., 2014), where dextral strike-slip and/or transpressional earthquakes take place. Other regional transfer zones developed along N-S Paleozoic-Mesozoic normal faults, such as the Sabz Puzhan dextral strike-slip fault (Lacombe et al., 2006), and the Izeh Fault (Sherkati and Letouzey, 2004; Lacombe et al., 2006; Ahmadhadi et al., 2007).

The Sarvestan area, a flat triangular area bounded by high-elevation anticlines (Fig. 2), hosts another major transfer zone: the Sarvestan Fault. The High Zagros Fault, delimiting to the north the Sarvestan Plain, is displaced to SE along the Sarvestan

Fault, which bounds the plain to the east. In this work we develop a geological model for the Sarvestan area, constrained by surface (geological mapping) and subsurface (well stratigraphies) geological data, by a network of 22 seismic lines, thermal maturity data and thermal modelling. This multidisciplinary set of data allowed us to define a geological evolution controlled by Paleozoic-Mesozoic rift-related extensional faulting, Cretaceous obduction of ophiolites, Tertiary normal faulting, salt tectonics, early syn-collisional basin inversion and multi-stage contractional tectonics. It is concluded that, although located in the so-called Zagros Simply Folded Belt, the Sarvestan area is actually complex in terms of geometry, stratigraphy and tectonics.

2. Geological setting

The Zagros belt developed from the collision and post-collisional convergence between Arabia and Iran (Navabpour and Barrier, 2012). In recent reconstructions, the collision occurred diachronously between the late Eocene and Oligocene, after the consumption of the Tethyan oceanic realm (Agard et al., 2005, 2011; Mouthereau et al., 2012). Convergence rates between Arabia and Eurasia were constrained to 2–3 cm/yr in a N–S direction in the last 10 My and are continuing today (Vernant et al., 2004). The Zagros orogen consists of different tectonostratigraphic realms (Fig. 1). From internal (NE) to external (SW) parts, these are the Sanandaj-Sirdjan zone, and the Urumieh-Dokhtar magmatic arc, separated by the Main Zagros thrust from the Imbricate zone (or High Zagros or Crash zone), in turn separated by the High Zagros thrust from the Simply Folded Belt Zagros foreland basin (e.g., Falcon, 1974; Stocklin, 1968).

The Zagros simply folded belt, where the Sarvestan area is located, is characterized by the superimposition of thin-skinned and thick-skinned tectonics (Mouthereau et al., 2007). Contractional tectonics deformed the Neoproterozoic? /Cambrian-Miocene successions of the rifted continental margin of the Arabian plate and Miocene-Recent foreland basin deposits (Fig. 3; Stocklin, 1968; Koop and Stoneley, 1982). Crustal scale cross-sections across the Zagros (Sherkati et al., 2006; Mouthereau et al., 2007), wells and subsurface data reveal a pile of stacked thrust sheets, constituted by sedimentary successions up to 12 km thick (Alavi, 2004).

The Fars region of the Zagros simply folded belt is located east of the N-S Kazerun transfer zone, a dextral strike-slip and/or transpressional fault (Sepehr and Cosgrove, 2005). In this region, the Precambrian basement rocks were unconformably overlain by up to 2000 m thick evaporites (halite and anhydrite) and gray trilobite-bearing dolostones with interlayered mafic and acidic volcanic rocks (Neoproterozoic?/ Cambrian Hormuz series; Falcon, 1974; Sepehr and Cosgrove, 2005). The Ordovician-Carbonifeorus mainly clastic rocks are poorly known owing to the paucity of outcrops and to the occurrence of major regional unconformities associated with Paleozoic erosional episodes (Alavi, 2004). Thickness and facies changes are also likely associated with Cambrian salt diapirism, basement faulting and sea level changes (Berberian and King, 1981). The Permian-Triassic succession mainly consists of carbonate rocks deposited in shallow marine environment containing also volcanic rocks related to the Permo-Triassic rifting and to the opening of the Neo-Tethys ocean (Alavi, 2004). After this rifting episode, sedimentation occurred in shallow water environments until Late Cretaceous times (Berberian and King, 1981). Late Cretaceous sedimentation in most of the Zagros was characterized by neritic carbonate sedimentation followed by deeper water conditions (marls and shales).

During Cenozoic time, sedimentation changed from open marine (shales and marls) to shallow water (e.g., Nummulites-bearing limestone) to continental (Miocene to Pleistocene post-collision clastic transgressive Mishan, Agha Jari and Bakhtiari Fms) environment.

In the Fars, low topography slopes (Talbot and Alavi, 1996), and symmetrical anticlines with no clear fold vergence have been interpreted as the evidence for a ductile decollement, provided by the Cambrian Hormuz Fm (Davis and Engelder, 1985; Cotton and Koyi, 2000). No other significant decollement levels were recognized to be active in the Fars, except for the coastal areas where the Triassic evaporites of the Dashtak Fm acted as an additional deep decollement (Sherkati et al., 2006; Motamedi et al., 2012; Najafi et al., 2014). No significant deformation gradient has been proposed to occur between internal and external zones of the belt, as suggested by the constant ratio between maximum folds amplitude and fold wavelength (Mouthereau et al., 2007).

The Arabian passive margin developed onto the former Hercynian orogeny by middle Permian-Triassic extensional tectonics (Koop and Stoneley, 1982; Navabpour et al., 2010). These thick-skinned extensional faults produced several NW-SE trending grabens, i.e., parallel to the current orientation of the belt contractional structures (Sepher and Cosgrove, 2004), in an oblique rift zone associated with the Neo-Tethys opening. However, a N-S trending set of faults, i.e., oblique to the direction of convergence, has been also recognized (Talbot and Alavi, 1996). This thick-skinned phase was followed by a Mesozoic thin-skinned phase, with the sedimentary cover affected by successive extensional structures and block tilting (Navabpour et al., 2010). Extensional tectonics probably continued during the early Tertiary but, in the late Cretaceous (Campanian), the external passive margin of the Arabian plate was affected by the southwestward obduction of a Neo-Tethyan ophiolite – radiolarite nappe (Béchennec et al., 1990; Breton et al., 2004).

The timing of shortening in the Fars was constrained by magnetostratigraphy studies on growth strata from clastic continental sequences (Khadivi et al., 2010; Ruh et al., 2014). These studies concluded that contractional deformation started in the proximity of the High Zagros fault in the Middle Miocene and propagated southward, reaching the Central Fars in the early Pliocene, with a migration rate of ca. 1 cm/yr.

2.1 The Sarvestan area

The Sarvestan plain is a flat triangular area with an average elevation of 1500 m asl. In this area, the rock substratum is covered by fluvial and lacustrine deposits, with the exception of a few scattered outcrops at the hinge of buried anticlines (Fig. 2). The plain is bounded to the north by the Ahmadi anticline, to the east by the Sarvestan fault zone and the Meyan anticline and to the south by the Quarau anticline. These anticlines are elevated some 1300-1400 m above the plain.

2.1.1 Sarvestan stratigraphy

The stratigraphy of the Sarvestan area is similar, for the Permian-Middle Cretaceous times to that of the remaining Fars region, showing a trend of gradual subsidence associated with marine ingressions that drove to a change in sedimentation from dominantly Palaeozoic clastics to Permian, Mesozoic and Tertiary carbonates (Powers 1968; Koop and Stoneley, 1982). Permian carbonates are interfingered with basaltic flows.

During the Early Triassic, the shallow marine carbonates of the Kangan Fm were deposited (Szabo and Kheradpir 1978), followed by the Middle Triassic evaporites of the Dashtak Fm during a regression stage (Berberian & King 1981) and by the Late Triassic shallow-water platform carbonates of the Khaneh Kat Fm (Pyriaei et al., 2010). The Early Jurassic was characterized by sedimentation of terrigenous clastic and transitional terrigenous to open marine deposits of the Neyriz Fm (Szabo and Kheradpir 1978), followed by the limestones and marls of the Khami Group (Surmeh, Fahliyan, Gadvan, Daryan; Middle Jurassic-Aptian). In the internal Fars, siltstones and iron/glauconite rich sandstones found in the upper parts of the Fahliyan and Dariyan Fms suggest regression, emergence and erosion in Neocomian and Late Aptian times (Navabpor et al., 2010). The shallow marine shales and carbonates of the Bangestan Group (Kazhdumi and Sarvak Fms; Albian– Turonian) contain also Late Turonian conglomerates and breccias, indicative of tectonic activity (Berberian & King 1981) and are the last sediments deposited in a typical passive margin environment.

The Late Cretaceous sedimentation in the Sarvestan area is complex owing to the occurrence of the southwestward obduction of ophiolites (e.g., Breton et al. 2004), which caused significant variations in sedimentary facies, sedimentation patterns and accommodation space, and shift of depocentres, as constrained by surface (stratigraphic sections) and subsurface (wells) data (Pyriaei et al., 2010). The obducted ophiolites crop out some tens of km north of Sarvestan zone.

Pelagic basinal marly facies (Gurpi Fm) were deposited in the Late Santonian–Maastrichtian. However, since Maastrichtian time, marly sedimentation (Gurpi Fm) in the SE part of the Sarvestan area was synchronous with rudist-dominated platform carbonate sedimentation (Tarbur Fm; Setudehnia 1972; Vaziri-Moghaddam et al.,

2005) in the central and northern Sarvestan area. This lateral facies change has been proposed to be caused by the uplift associated with the emplacement of the ophiolites (Pyriaei et al., 2010). Uplift and tectonic activity in Late Cretaceous times are also suggested by frequent calciturbiditic beds in Maastrichtian deposits.

The Tarbur carbonates were overlain by Maastrichtian-Paleogene evaporitic facies (Sachun Fm), consisting of gypsiferous limestones, dolostones (with bird's eyes and salt clasts) and red marls deposited in a sabkha environment. Heteropic to the Sachun evaporitic limestones were the neritic shales and marls of the Pabdeh Fm, deposited on top of the Gurpi basinal sediments. During the Eocene-Oligocene, shallow water limestones (Jahrum and Asmari Fms) were deposited onto the entire area and were overlain, in Early Miocene times, by supratidal sabkha-like deposits (Razak Fm), followed, in Middle Miocene times, by marls (Mishan Fm), red beds (Agha Jari Fm) and by Late Miocene molasse-type conglomerates (Bakhtiari Fm). The Middle Miocene clastic sedimentation marks the transition of the Sarvestan area to a foreland basin setting. According to Khadivi et al. (2010), a magnetostratigraphic correlation with chron C6n dates the bottom of the Razak Fm to 19.7 Ma. The transition to the Agha Jari Fm is correlated with chron C5Cn, at 16.6 Ma. The onset of deposition of the Bakhtiari conglomerates correlates with the chron C5AD, at approximately 14.8 Ma (Khadivi et al., 2010).

2.1.2 Sarvestan evolution

The Permian-Mesozoic extensional tectonics of the internal parts of the Fars region was studied by Navabpour et al. (2010). Although the Permian-Early Triassic extensional tectonics cannot be reconstructed in detail, owing to the scattered and poor-quality nature of outcrops, the beginning of rifting (N-S extension) between the Iranian and Arabian continental plates is generally ascribed to this time span, based on the occurrence of Permian basalts and on the recognition of syn-depositional normal faults in seismic lines across the Dezful area (Sepehr & Cosgrove 2004) and in outcrops in Oman (Chauvet et al. 2009). In the vicinity of the Sarvestan area, syn-depositional extensional faults were active in Middle-Late Triassic (Khaneh Kat Fm), Middle-Late Jurassic (Surmeh Fm), Aptian (Dariyan Fm), Cenomanian-Turonian (Sarvak Fm) and Campanian-Maastrichtian (Gurpi Fm) times (Navabpour et al., 2010). Little evidence of syndepositional normal faulting was found in the Eocene Pabdeh Fm. Two main directions of extension, i.e., N-S, producing E-W trending faults and NE-SW, associated with NW-SE trending fault, were recognized.

The onset of collision in the internal Fars has been proposed to have occurred in late Oligocene-Early Miocene times (Agard et al. 2005; Sherkati et al. 2005). The onset of folding in an area NW of Sarvestan (Chahar-Makan syncline) has been recently constrained by magnetostratigraphic dating of growth strata to 15-14 Ma (Khadivi et al., 2010).

The Sarvestan fault (Berberian and Tchalenko, 1976), with a length of about 90 km, has a NNW-SSE strike and is roughly parallel to the Kazerun fault (Fig. 1). It has been inferred to be a strike-slip fault owing to strike-slip basement earthquakes developed on parallel faults (Karebass and Sabz Pushan) and to the apparent 20 km right-lateral offset of the Ahmadi anticline (Berberian, 1995; Lacombe et al., 2006). Two Hormuz salt domes were intruded along the fault (Fig. 2). However, compressional activity along this fault is indicated by the occurrence of the Meyan anticline, parallel to the fault, suggesting a noticeable amount of fault-perpendicular shortening (Lacombe et al., 2006). Molinaro et al. (2005) proposed that the Sarvestan fault acquired a surface expression only during the late evolution of the Zagros simply folded belt, in association with basement-involved shortening. Lacombe et al. (2006) proposed that the Sarvestan fault behaved as a local transfer fault during folding of the sedimentary cover.

No direct seismic evidence associated with motion along the Sarvestan fault has been recorded (Berberian, 1995). However, the 1890 March 3rd Ms 6.4 earthquake (Ambraseys and Melville, 1982), possibly nucleated along the Sarvestan fault (Berberian, 1995). Recent activity along the fault has been inferred also from quantitative geomorphological studies (Dehbozorgi et al., 2010). No significant present-day activity has been highlighted by GPS studies (Hartzfeld et al., 2010).

In the Sarvestan area, commercial oil was found in the Sarvak reservoir. Oil was generated either from a Garau-type basinal facies developed in the interval between the upper part of the Surmeh Fm and the base of the Khami Group, or more probably, from the Kazhdumi Fm (Bordenave, 2008).

3. A 3D model of the Sarvestan area

3.1 Geological constraints

The seismic profiles (see Fig. 2 for their location) were interpreted and depth converted and the geological cross sections were built using 3DMove 2014 software by Midland Valley (http://www.mve.com/software/move). The cross sections were constrained by surface and subsurface geological data, geophysical data and are consistent with thermal maturity data and thermal modelling.

The surface geological data were taken from the following 1:100.000 sheets of the Geological Map of Iran: Kangan (no. 20867W), Kushk (no. 6647) and Sarvestan (no. 6648). Stratigraphic sections from NIOC (National Iranian Oil Company) internal reports were also used. For the deeper parts of the succession, not covered by borehole stratigraphies and surface stratigraphic sections, information on thickness and facies of sediments were taken from the paleogeographic maps of Koop and Stoneley (1982) and Pyriaei et al. (2010) and from the review of Alavi (2004). Finally, geological observations and data acquired during a 2012 field campaign were used to integrate published data.

Subsurface geological data consist of the following borehole stratigraphies: Sim-1 well, Sarvestan-1 and Sarvestan-3 wells. The stratigraphy of the area south of the Sarvestan plain was built using the stratigraphy of the Sim-1 well. The stratigraphy of the Sarvestan Plain is constrained by Sarvestan-1 and Sarvestan-3 wells. The stratigraphy of the area north of the Sarvestan Plain is not constrained by wells available to the authors. The stratigraphy was reconstructed using the paleogeographic maps of Koop and Stoneley (1982) and Pyriaei et al. (2010).

Geophysical data consist of 22 unpublished seismic lines acquired by NIOC through the Sarvestan Plain. Four sections are parallel to the NW-SE trend of the Zagros anticline axes, and 13 are perpendicular to the regional structural trend and the remaining sections are oblique to the regional trend. The seismic lines have a total length of around 300 km and were calibrated using the Sarvestan-1 and Sarvestan-3 well stratigraphies.

The geometry of the structures buried below the Sarvestan plain were reconstructed in map view interpolating top-Asmari and top-Tarbur reflectors (Fig. 4 and 5) with the kriging algorithm of 3DMove software. To link buried and outcropping structures in geological cross sections (Fig. 6), depth conversion was performed using a constant velocity of 4500 m/s, consistent with regional findings.

3.2 A description of the main structural features

The structures buried beneath the plain and those bounding it are completely different. A first difference concerns structures orientation. Below the plain, the orientation of folds axes, reconstructed by the seismic data are constantly oriented E-W (Fig. 4 and 5). The structures at the plain boundary have variable orientations, ranging from the regional NW-SE to WNW-ESE trending of the Zagros (Quarau anticline) to E-W (and Ahmadi anticline) to NNE-SSW (Meryan anticline) directions. Also the tectonic style is very different. The structural elevation of the anticlines buried below the plain is some 2000-3000 m lower than that of the cropping anticlines. In addition, the anticlines below the plain have rather open geometries and are not associated with major thrust faults, whereas the anticlines bounding the plain are associated with major thrust or transpressional faults on both sides. Finally, the anticlines below the plain are rather symmetric, whereas the cropping anticlines show marked asymmetry (Figs. 2, 6 and 7). The Ahmadi anticline has a more steeply dipping southern flank (bedding dip up to 60-70°), indicating a S-vergence, but shows no overturned bedding attitude. The Quarau anticline has a steeply dipping to overturned NE flank, indicating a NE-vergence, opposite to the regional (SW-ward) vergence of the simply folded Zagros belt. The Meyan anticline displays a very steep to overturned western flank, suggesting a W-vergence.

The characteristics of the faults associated with these anticlines are very different. The Kahdan and Quarau faults bound the Quarau anticline respectively to the NE and SW.

The Kahdan fault is the major thrust fault and displays Asmari Fm rocks in the hanging wall and Razak Fm marls in the footwall. The overturned strata in the NE flank of the fault suggest a fault propagation nature for the Kahdan fault and, according to this interpretation, the top-to-NE kinematics indicate that this fault is a major regional backthrust. Alternatively, the geometry of the fault could be explained invoking a thrust fault cutting through an already overtuned flank of a detachment fault (for similar structures in the Zagros see Sherkati et al., 2005 and Verges et al., 2011). The Quarau fault displays a ramp-and-flat geometry (Fig. 6 and 8c) and, even more importantly, was characterized by slip after the deposition of the Bakhtiari Fm (Asmari Fm in the hangingwall and Bakhtiari Fm in the footwall (Figs. 2 and 8b). Both faults change their direction from NW-SE to EW in the SE hinge of the Sarvestan plain, suggesting again a control by inherited structures. The Ahmadi anticline is bounded by the Maharlu fault to the south. This fault bears Razak Fm rocks in the hanging wall and Agha Jari Fm rocks in the footwall and has a ENE-WSW to E-W direction, with the exception of the easternmost part, where it rotates to NW-SE direction and likely merges with the Sarvestan fault. The fault bounding the northern limb of the Ahmadi anticline has a ENE-WSW direction, also rotates to NW-SE direction in the eastern part and displays a small displacement (Razak Fm in both hanging wall and footwall). The Sarvestan fault is a major dextral transpressional lineament. In the literature, the Meyian anticline has been interpreted as the continuation of the Ahmadi anticline (Berberian, 1995). If this interpretation is true, the dextral lateral displacement can be constrained to some 20 km. In our view, however, this interpretation is not fully straightforward, provided that the two anticlines have different geometries and axes directions. It is however straightforward the interpretation of dextral strike-slip component of motion, as indicated, among others, by the anticlines north of the Khethabad fault, that are rotated along the Sarvestan fault.

The Sarvestan fault bifurcates around the Kuh-e-Namak salt dome and south of the Meyan anticline, where other salt plugs crop out. It is difficult to constrain the age of diapirism in this region. The youngest rocks pierced by diapirs are the Asmari Fm limestones. This suggests a post Asmari Fm activity but does not preclude earlier stages. Two minor splays, oblique to the main fault, likely characterized by transpressional kinematics with a prevailing reverse component, occur also in the central part of the fault (close to the sampling site SAC1). The Sarvestan fault, south of the Meyan anticline shows a horse-tail organization and rotates from NNW-SSE to NW-SE direction. The fact that the Sarvestan fault could connect with the Maharlu thrust and continues as a thrust fault south of the Meyan anticline suggests that it may have operated as a strongly oblique ramp of the Maharlu thrust fault system. It is emphasized that the Sarvestan fault displays the largest offset recognised in the faults of the study area, with Sarvak Fm rocks in the hanging wall and Asmari/Razak rocks in the footwall. This is counterintuitive for a transpressional fault or for a strongly oblique ramp. The Meyan anticline is bounded to the NE by the Meyan Jangal fault, again a dextral traspressional fault subparallel to the Sarvestan fault.

The Meyan anticline deserves further discussion. It has a structural elevation (measured on the top Tarbur Fm) some 4000 m higher than the Sarvestan plain structures. This is the highest elevation in the area. By contrast, it is characterized by a very small lateral continuity (around 20 km), compared to that of the Quarau and Ahmadi anticlines (40-50 km long). Most probably, a part of the structural elevation is due to diapirism. The core of the anticline (i.e., the area where the Gurpi and Sarvak Fms crop out) had a lens shape and is elongated parallel to the Sarvestan fault.

Both shape and dimensions recall that of the Kuh-e-Namak diapir. Differently from this diapir, the Cambrian salt beneath the Meyan anticline did not reach the surface. Besides the described structures, a major feature observed in the region is the angular unconformity between the slightly folded Agha Jari sandstones and the Bakhtiari conglomerates, east of the Kuh-e-Namak salt plag (Fig. 8a). This stratigraphic boundary constrains the occurrence of folding and uplift prior to the deposition of the Bakhtiari Fm conglomerates. Another fundamental observation to constrain the age of shortening in the area is the fact that the Bakhtiari conglomerates are involved in thrusting and strongly folded (for example in the syncline south of the Maharlu fault), indicating that shortening occurred also after the deposition of this formation. These ages of shortening will be used as constraints for the thermal modelling.

4. Thermal constraints

4.1 Methods

Clay minerals in shales and sandstones undergo diagenetic and very low-grade metamorphic reactions in response to sedimentary and/or tectonic burial. Reactions in clay minerals are irreversible under normal diagenetic and anchizonal conditions, so that exhumed sequences generally retain indices and fabric indicative of their maximum maturity and burial. One of the parameters generally used to provide information on thermal evolution of sedimentary successions is the variation in composition and stacking order of mixed layered minerals. In particular, mixed layers illite-smectite (I-S) are widely used in petroleum exploration as a geothermometer (Pollastro, 1990; Aldega et al., 2014) and, thus, as indicators of maximum burial conditions of sedimentary sequences in fold-and-thrust belts (Aldega et al., 2007; 2011; Caricchi et al., 2015; Corrado et al., 2010; Di Paolo et al., 2014; Izquierdo-Llavall et al., 2013). The identified changes comply with the following scheme of progressive thermal evolution: di-smectite - disordered mixed layers (R0) - ordered mixed layers (R1 and R3) - illite - di-octahedral K-mica (muscovite).

X-ray diffraction analyses were carried out with a Scintag X1 X-ray system (CuKα radiation) at 40 kV and 45 mA. Oriented air-dried and ethylene-glycol solvated samples of the <2 μm (equivalent spherical diameter) grain-size fraction were scanned from 1 to 48 °2θ and from 1 to 30 °2θ respectively with a step size of 0.05 °2θ and a count time of 4 s per step. The illite content in mixed layers I-S was determined according to Moore and Reynolds (1997) using the delta two-theta method after decomposing the composite peaks between 9-10 °2θ and 16-17 °2θ. The I-S ordering type (Reichweite parameter, R; Jagodzinski 1949) was determined by the position of the I001-S001 reflection between 5 and 8.5 °2θ (Moore and Reynolds 1997). Peaks in relative close position were selected for clay mineral quantitative analysis of the <2 μm grain-size fraction in order to minimize the angle-dependent intensity effect. Composite peaks were decomposed using Pearson VII functions and the WINXRD Scintag associated program. Integrated peak areas were transformed into mineral concentration by using mineral intensity factors as a calibration constant (for a review, see Moore and Reynolds 1997).

4.2 Results

A suite of 11 samples, belonging to the Upper Cretaceous-Miocene portion of the Fars sedimentary succession, has been collected in the hanging wall and footwall of the Sarvestan fault (Tab.1).

X-ray semi-quantitative analysis shows that sediments younger than the Paleocene are characterized by the occurrence of palygorskite which is absent in older rocks. The Agha Jari Fm is composed of illite (51%), chlorite (35%), mixed layer I-S (9%) and palygorskite (5%).

The Razak Fm is mainly constituted by an illite-rich composition with subordinate amounts of chlorite, kaolinite and mixed layers I-S. The underlying Sachun Fm displays palygorskite or illite as major component of the <2 µm grain-size fraction, mixed layer I-S and minor amounts of chlorite (<3%). Marls of the Pabdeh Formation are made up of random ordered mixed layers I-S (53%), illite (34%), kaolinite (6%) and chlorite (7%).

In the Gurpi Fm, clay minerals assemblage depends on the sampled lithology. Marls (GUR4, GUR5) are composed of mixed layer I-S, illite and kaolinite whereas pelites (GUR3) are mainly constituted by mixed layered clay minerals such as chlorite-smectite (C-S) and I-S, illite and subordinate amounts of kaolinite and chlorite.

Temperature dependent clay minerals display low levels of thermal maturity. In particular, we observe an increase of the illite content in mixed layer I-S as function of stratigraphic age (depth) in the hanging wall units. Random ordered I-S (R0) with high expandability (30-45% of illitic layers) which characterize the Miocene deposits convert into short range ordered structures (R1) with an illite content of 60-70% in the Late Cretaceous Gurpi Fm indicating early to late diagenetic conditions. This transition suggests the occurrence of temperatures in the range of 100-110 °C (Hoffman and Hower, 1979; Pollastro, 1990).

In the footwall units, samples belonging to the Razak and Sachun Fms show higher levels of thermal maturity than those recorded by deposits of similar age cropping out in the fault hanging wall. Mixed layer I-S are short range ordered structures with an illite content of 60-70% indicating the first stages of the late diagenetic zone.

4.3 Burial and thermal Models

Simplified reconstructions of the burial and thermal history of the sedimentary successions cropping out across the Sarvestan fault have been performed using the software package Basin Mod 1-D (1996; Fig. 9).

The main assumptions for modeling are that: (1) rock decompaction factors apply only to clastic deposits, according to Sclater and Christie's method (1980); (2) seawater depth variations in time are not relevant in modeling, because thermal evolution is mainly affected by sediment thickness rather than by water depth (Butler, 1992); (3) thermal modeling is performed using LLNL Easy %Ro method based on Sweeney and Burnham (1990); and (4) a geothermal gradient of 20°C/km and a surface temperature of 20°C were adopted.

Thicknesses have been calculated from field mapping and well data and ages are from literature. In particular, ages for syn-orogenic foreland sediments are from Khadivi et al. (2010) and those of pre-orogenic sediments are from sheet nr. 6648 of geological map of Iran (1:100000).

The burial history of the sedimentary succession cropping out at the hanging wall of the Sarvestan fault, was constrained by mixed layered clay minerals data (Tab. 1; Figs. 9A and C). The reconstructed evolution begins in Cretaceous time with the deposition of about 500 m-thick sediments of the Sarvak Fm in neritic environment

(Fig. 9A). The Late Cretaceous sedimentation was followed by deeper water conditions with deposition of marls and shales of the Gurpi Fm (about 300 m) and evolved to shallow-water marine environments in Maastrichtian times. The Gurpi Fm graded up to thick-bedded to massive anhydritic limestones of the Tarbur Fm (500 m). During Paleocene times, red shale and evaporites of the Sachun Fm deposited in the Sarvestan area with thicknesses of about 300 m. Sabhka-like conditions persisted until Oligocene times, and the Sachun Fm graded up and interfingered with dolostones of the Jahrum Fm in the Eocene and evolved to shallow marine Nummulites-bearing limestones of the Asmari Fm in the Oligocene.

From early Miocene onwards, sedimentation rates increased and a large amount of marls and siliciclastic rocks (Razak and Agha Jari Fms) buried the Sarvak Fm at depths of ~3.6 km.

During the Serravallian, the succession was uplifted and the Agha Jari Fm partially eroded (about 200 m) as a consequence of the advancement of compressional front and siliciclastic deposits of the Bakhtiari Fm sedimented in depozones (Fig. 9B). This is consistent with the occurrence of the angular unconformity between the Agha Jari and Bakhtiari Fms (Fig. 8a). At the time of maximum burial (early Pliocene), Paleocene to Miocene deposits were thermally immature whereas Cretaceous rocks of the Gurpi and Sarvak Fms entered the early mature stage of hydrocarbon generation (Fig. 9B). This reconstruction foresees the erosion of 400 m-thick Bakhtiari Fm since early Pliocene times and indicates that sedimentary load was the main factor affecting levels of thermal maturity. The type of evolution outlined here represents the best calibration against illite content in mixed layer I-S data, as shown by the resulting maturity curve of figure 9C.

The burial reconstruction of the sedimentary succession at the fault footwall displays a different evolution during the Miocene (Fig. 9D) as siliciclastic deposits present higher levels of thermal maturity than those observed in deposits of similar age in the hanging wall (Tab. 1, Fig. 9G).

Two alternative scenarios match clay mineralogical data. The first scenario considers high sedimentations rates since early Miocene (Fig. 9E), the second accounts for thrust tectonics as an important factor affecting thermal maturity data (Fig. 9F).

In the burial history of Figure 9E, the increase of siliciclastic input during the early Miocene (about 1700 m of Razak and 2000 m of Agha Jari Fms) has been related to the mobilization of the Cambrian salt in the proximity of the Sarvestan fault. Salt diapirism caused enhanced subsidence in the footwall areas and greater accommodation space where siliciclastic rocks could accumulate. Since the Serravallian, the advancement of the orogenic front uplifted the area and erosion began to remove the lithostatic load. While erosion worked in more structurally elevated areas of the fault footwall, the Bakthiari Fm sedimented in depozones located at the hanging wall areas.

The second scenario (Fig. 9F) foresees the coupled effect of salt diapirism and thrust tectonics to explain the higher thermal maturity data observed at the fault footwall. After sedimentation of 1100 m-thick sediments of the Agha Jari Fm, the succession was tectonically buried by a 900 m-thick thrust sheet, now completely eroded. Either sedimentary or tectonic load buried the Sarvak Fm at depths of 5.4 km in middle Miocene times. At that time, the Sarvak Fm experienced middle mature stages of hydrocarbon generation whereas Late Cretaceous to early Miocene rocks underwent early stages of hydrocarbon generation as indicated by the thermal maturity curve of Fig. 9G.

In both scenarios, burial reconstructions account for an erosion of 3000 m-thick succession: 500 m during the Serravallian uplift at a rate of 0.052 mm/yr and 2500 m since early Pliocene times with an erosion rate of 0.47 mm/yr.

5. Tectonic and stratigraphic evolution

Although there are no direct evidence from facies and/or thickness changes in the sedimentary cover in the study area, on the base of Permian and Late Jurassic isopach maps by Koop and Stoneley (1982), the present day Sarvestan fault likely was a NNW-SSE trending Paleozoic-Mesozoic rift-related normal fault dipping to the east (Fig. 10). The occurrence of NNW-SSE rift related extensional faults was described in adjacent regions by Navabpour et al. (2010). This geometry is consistent with the larger advancement of the thrust front (Fig. 2) associated with a thicker sedimentary pile to the east of the fault, in agreement with analogue models (Huiqi et al., 1992). A similar interpretation has been proposed for similarly oriented transfer zones in the Fars, such as the Kazerun (Sepehr and Cosgrove, 2005) and the Sabz-Pushan (Lacombe et al., 2006) faults.

Furthermore, the occurrence of E-W trending compressional structures at depth in the Sarvestan plain, with different attitude from the regional axial trend, suggests the presence of inherited extensional structures in agreement with recent regional findings (Navabpour et al., 2010). We propose that the activity of a set of normal faults subparallel to the Quarau fault (see section 4 in Fig. 6), lowered, in Tertiary time (Fig. 10), the present day Sarvestan area, as constrained by the abrupt change of stratigraphy when entering the Sarvestan plain, characterized by thicker Tertiary successions with respect to outer areas. Unfortunately, the area where such faults should be located (the Quarau anticline) is not covered by the seismic lines used in this work. Alternative hypotheses that do not consider the occurrence of Tertiary extensional faults, such as incresaed subsidence associated with thrust or subduction flexure (as successfully proposed for the Lurestan area by Emami et al., 2010), would imply a progressive thickening of Tertiary sediments, at odds with stratigraphic evidence.

The obduction of ophiolites in the Late Cretaceous (Breton et al., 2004), cropping out some tens of km north of the study area, controlled basin geometry and sedimentation environment. Prior to the Late Cretaceous, deep-water facies were deposited in the Sarvestan area and shallow water carbonates to the south of it. On the contrary, in Late Cretaceous time, the Sarvestan area was characterized by sedimentation of shallow water carbonates of the Tarbur Fm, whereas to the south, deeper water marls of the Gurpi Fm were heteropically deposited (Piryaei et al., 2010). Since the Paleocene, sedimentation environment and subsidence rate were similar over the entire area while the Jahrum Fm were sedimenting.

The onset of shortening in the Early Miocene highlights different thermal evolution of the sediments in the hanging wall and footwall of the Sarvestan fault. As discussed in the previous section, the higher thermal maturity of sediments at the fault footwall can be explained either in terms of higher subsidence (enhanced by salt tectonics) and faster sedimentation or by tectonic loading (overthrusting). Both scenarios lead to a thermal evolution consistent with thermal maturity data. No overthrusts (or remnants of them) and no significant subduction-related normal faults were observed in the seismic lines and in the field. This suggests that a fault-related origin for explaining thermal maturity data at the Sarvestan fault footwall is unlikely. The higher subsidence in the Sarvestan fault footwall is instead explained by a flow of Cambrian salt from the plain area towards the hanging wall of the Sarvestan fault, where salt diapirism occurred during the deposition of the Lower-Middle Miocene Razak and Agha Jari Fms. Salt tectonics is invoked also to explain, at least in part, the development of the Meyan overturned anticline in the hanging wall of the Sarvestan fault.

An early phase of contractional deformation occurred in the Middle Miocene (since 15 Ma; Fig. 10), after the deposition of the Agha Jari Fm generating the E-W oriented folds buried below the plain, likely inverting inherited normal faults, and folds in the hanging wall of the Sarvestan fault. This interpretation is supported by the different orientations of the folds buried under the Sarvestan plain, which suggest a strong control of pre-existent faults on contractional deformation. This early shortening phase, associated with uplift and erosion, is supported by the angular unconformity between the Agha Jari and Bakhtiari Fms (Fig. 8a). The erosion of these structures led to the deposition of the Bakhtiari Fm conglomerates in Middle-Late Miocene times. A localized load in the footwall favored the localization of deformation and the later development of thrust faults and anticlines bounding the Sarvestan plain (Bigi et al., 2010). This reconstruction is supported by the emplacement of the Asmari limestones onto the Bakhtiari conglomerates along the Quarau fault (Figs. 2 and 8b). Far to the north, this contractional event is confirmed by the occurrence of an exposed Bakhtiari syncline, at the footwall of the Maharlu fault (Fig. 2). Late Miocene time for this deformation (6-5 Ma; Fig. 10) is constrained by thermal models (Fig. 9D) as the minimum time interval necessary to achieve the thermal maturity levels of the Razak Fm at the footwall of the Sarvestan fault. The low elevation of the Sarvestan plain suggests that, during this stage, the buried structures were not significantly reactivated. The Sarvestan dextral transpressional fault, that likely acted as a strongly oblique ramp of the Maharlu thrust, mainly structured in this period, although its activity may have continued until present, as inferred from seismicity.

6. Conclusions

Although located in the simply folded Zagros, surface and subsurface geological data, seismic lines, thermal maturity data and 1D thermal modelling indicate that the Sarvestan area is a region of high geometric complexity, which is the result of a comparatively complex geological evolution.

Below the Sarvestan plain, open folds, with E-W axes, were recognized buried by alluvial sediments. These folds have different orientations with respect to the high elevation folds bounding the plain (the NW-SE to WNW-ESE trending Quarau anticline, the E-W Ahmadi anticline and the NNE-SSW Meryan anticline), which are characterized by structural elevations some 2000-3000 higher than the buried anticlines. The high elevation anticlines are bounded on both sides by thrusts or transpressional faults, parallel to the fold limbs, and a major backthrust is recognized at the SW boundary of the Sarvestan plain.

Thickness and facies changes in the sedimentary cover were controlled by E-W and NNW-SSE trending normal faults during the Paleozoic to early Tertiary and by the Cretaceous obduction of ophiolites. Miocene deposits in the Sarvestan areas show different levels of thermal maturity. The higher thermal maturity in the present-day footwall of the Sarvestan fault is explained by high subsidence due to flow of Cambrian salt, associated with diapirism, from the footwall to the hanging wall area, in Early-Middle Miocene times (between 19.7 and 15 Ma).

An early phase of contractional deformation occurred in the Middle Miocene (since 15 Ma) generating the E-W oriented folds buried below the plain, likely inverting inherited normal faults, and tilting of strata also to the east of the Sarvestan plain. The erosion of these structures was followed by the unconformable deposition of the Bakhtiari Fm conglomerates in Middle-Late Miocene times. A later phase of contractional tectonics generated the thrust faults and the anticlines bounding the Sarvestan plain in Late Miocene time (some 6-5 Ma ago). During this stage the Sarvestan dextral transpressional fault started to develop as a strongly oblique ramp of the Maharlu thrust.

Acknowledgements

Financial support from the Darius Programme, from Progetti di Ateneo 2014 and PRIN2010/11 (Project 20107ESMX9 “Crisi e ripresa di sistemi carbonatici e potenziale per la formazione di reservoir: i ruoli di clima, tettonica e magmatismo”) to Eugenio Carminati is acknowledged. The National Iranian Oil Company is thanked for assistance in fieldwork organization and logistics and for allowing the publication of this work and of the associated data. Shahram Sherkati, Fabio Trippetta and Sveva Corrado are thanked for common work through the last years. Hossain Narimani and Fabio Trippetta are thanked for sharing the fieldwork campaign. Midland Valley is thanked for providing educational licence for Move software. The critical reading of two anonymous reviewer greatly improved the quality of this work.

References

Aldega, L., Corrado, S., Grasso, M., Maniscalco R., 2007. Correlation of diagenetic data from organic and inorganic studies in the Apenninic-Maghrebian fold-and-thrust belt: a case study from Eastern Sicily. The Journal of Geology, 115 (3), 335-353.

Aldega, L., Corrado, S., Di Paolo, L., Somma, R., Maniscalco, R., Balestrieri, M.L., 2011. Shallow burial and exhumation of the Peloritani Mts. (NE Sicily, Italy): Insight from paleo-thermal and structural indicators. Geological Society of America Bulletin, 123, 132-149.

Aldega, L., Corrado, S., Carminati, E., Shaban, A. & Sherkati, S., 2014. Thermal evolution of the Kuh-e-Asmari and Sim anticlines in the Zagros fold-and-thrust belt: implications for hydrocarbon generation. Marine and Petroleum Geology, 57, 1-13

Agard, P., Omrani, J., Jolivet, L., Mouthereau F., 2005. Convergence history across Zagros (Iran): Constraints from collisional and earlier deformation. Int. J. Earth Sci., 94(3), 401–419.

Agard, P., Omrani, J. Jolivet, L. Whitechurch, H., Vrielynck, B., Spakman, W., Monie, P., Meyer, B., Wortel, R., 2011. Zagros orogeny: A subduction-dominated process. Geol. Mag., 148(5–6), 692–725.

Ahmadhadi, F., Lacombe, O., Daniel, J.M., 2007. Early reactivation of basement faults in Central Zagros (SW Iran): evidence from pre-folding fracture populations in the Asmari Formation and Lower Tertiary paleogeography. In: Lacombe O., Lavé, J., Roure, F., Vergés, J. (eds) Thrust belts and foreland basins: from fold kinematics to hydrocarbon systems, Springer-Verlag, 205-228. doi: 10.1007/978-3-540-69426-7_11.

Alavi, M., 2004. Regional stratigraphy of the Zagros fold-thrust belt of Iran and its proforeland evolution. American Journal of Science 304, 1-20.

Allen, M.B., Talebian, M., 2011. Structural variation along the Zagros and the nature of the Dezful Embayment. Geol. Mag. 148:911-924. doi: 10.1017/S0016756811000318

Ambraseys, N.N., Melville, C.P., 1982. A History or Iranian Earthquakes. Cambridge Univ. Press, Cambridge, 219 pp.

Basin Mod® 1-D for WindowsTM, 1996, A Basin Analysis Modelling System version 5.4 Software: Denver, Platte River Associates, 386 p.

Béchennec, F., Le Meéour, J., Rabu, D., Bourdillon-Jeudy-De-Grissac, C., De Wever, P., Beurrier, M., Villey, M. 1990. The Hawasina Nappes: stratigraphy, palaeogeography and structural evolution of a fragment of the south-Tethyan passive continental margin. In: ROBERTSON, A. H. F., SEARLE, M. P. & RIES, A. C. (eds) The Geology and Tectonics of the Oman Region. Geological Society, London, Special Publications, 49, 213–223.

Berberian, M., 1995. Master “blind” thrust faults hidden under the Zagros folds: active basement tectonics and surface tectonics surface morphotectonics. Tectonophysics 241, 193–224.

Berberian, M., Tcahlenko, J., 1976. Earthquakes of the southern Zagros (lran): Bushehr region. Geol. Surv. Iran, 39, 343-370.

Berberian, M., King, G.C.P., 1981. Towards a paleogeography and tectonic evolution of Iran. Canadian Journal of Earth Sciences, 18, 210–265.

Bigi, S., Di Paolo, L., Vadacca, L., Gambardella, G., 2010. Load and unload as interference factors on cyclical behavior and kinematics of Coulomb wedges: Insights from sandbox experiments. Journal of Structural Geology 32, 28–44, doi:10.1016/j.jsg.2009.06.018

Bordenave, M.L., 2008. The origin of the Permo-Triassic gas accumulations in the Iranian Zagros foldbelt and contiguous offshore areas: a review of the Paleozoic petroleum system. J Petrol Geol, 31, 3-42, doi: 0.1111/j.1747-5457.2008.00405.x

Breton, J.P., Béchennec, F., Le Métour, J., Moen-Maurel, L., Razin, P., 2004. Eoalpine (Cretaceous) evolution of the Oman Tethyan continental margin: insights from a structural field study in Jabal Akhdar (Oman Mountains). GeoArabia, 9, 41 – 58.

Butler, R.W.H., 1992. Hydrocarbon maturation, migration and tectonic loading in the western Alps. In: England, W.A., Fleet, A.J., (Eds.), Petroleum Migration. Geological Society of London, Special Publications 59, 227–244.

Caricchi, C., Aldega, L., Corrado, S., 2015. Reconstruction of maximum burial along the Northern Apennines thrust wedge (Italy) by indicators of thermal exposure and modeling. Geological Society of American Bulletin, doi: 10.1130/B30947.1.

Carminati, E., Aldega, L., Bigi, S., Corrado, S., D’Ambrogi, C., Mohammadi, P., Shaban, A., Sherkati, S., 2013. Control of Cambrian evaporites on fracturing in fault-related anticlines in the Zagros fold-and-thrust belt. International Journal of Earth Sciences, doi: 10.1007/s00531-012-0858-0.

Carminati, E., Aldega, L., Trippetta, F., Shaban, A., Narimani, H., Sherkati, S., 2014. Control of folding and faulting on fracturing in the Zagros (Iran): the Kuh-e-Sarbalesh anticline case. Journal of Asian Earth Sciences, 79, 400-414, http://dx.doi.org/10.1016/j.jseaes.2013.10.018.

Chauvet, F., Dumont, T. and Basile, C., 2009. Structures and timing of Permian rifting in the central Oman mountains (Saih Hatat). Tectonophysics, 475, 563-574.

Corrado, S., Invernizzi, C., Aldega, L., D'Errico, M., Di Leo, P., Mazzoli, S., Zattin M., 2010. Testing the validity of organic and inorganic thermal indicators in different tectonic settings from continental subduction to collision: the case history of the Calabria-Lucania border (southern Apennines, Italy). Journal of the Geological Society, 167, 985-999.

Cotton, J.T., Koyi H.A., 2000. Modeling of thrust fronts above ductile and frictional detachments; application to structures in the Salt Range and Potwar Plateau, Pakistan. Geol. Soc. Am. Bull., 112. 351–363. doi: 10.1130/0016-7606(2000)112<351:MOTFAD>2.0.CO;2

Davis, D.M., Engelder, T., 1985. Role of salt in fold-and-thrust belts. Tectonophysics, 119, 67–88.

Dehbozorgi, M., Pourkermani, M., Arian, M., Matkan, A.A., Motamedi, H., Hosseini, A., 2010. Quantitative analysis of relative tectonic activity in the Sarvestan area, central Zagros, Iran. Geomorphology 121, 329–341.

Di Paolo, L., Olivetti, V., Corrado, S., Aldega, L., Balestrieri, M.L., Maniscalco, R., 2014. Detecting the stepwise propagation of the Eastern Sicily thrust belt (Italy): insight from thermal and thermochronologic constraints. Terra Nova, 26(5), 363-371.

Emami, H., Vergés, J., Nalpas, T., Gillespie, P., Sharp, I., Karpuz, R., Blanc, E.P., Goodarzi, M.G.H., 2010. Structure of the Mountain Front Flexure along the Anaran anticline in the Pusht-e Kuh Arc (NW Zagros, Iran): insights from sand box models. Geol. Soc. London, Spec. Publ. 330, 155-178.

Falcon, N.L., 1974. Southern Iran: Zagros Mountains, in Mesozoic-Cenozoic Orogenic Belts. Data for Orogenic Studies, edited by A. M. Spencer. Geological Society London Special Publications, 4, 199–211.

Hatzfeld, D., Authemayou, C., van der Beek, P., Bellier, O., Lavé, L., Oveisi, B., Tatar, M., Tavakoli, M., Walpersdorf, A., Yamini-Fard, F., 2010. The kinematics of the Zagros Mountains (Iran). In: Leturmy P, Robin C (eds) Tectonic and Stratigraphic Evolution of Zagros and Makran during the Mesozoic–Cenozoic. Geological Society London Special Publications, 330, 19–42. doi: 10.1144/SP330.3

Hoffman, J., Hower, J., 1979. Clay mineral assemblages as low-grade metamorphic geothermometers: application to the thrust faulted disturbed belt of Montana, USA. In Scholle, P. A., and Schluger, P. S., eds. Aspects of diagenesis. SEMP Spec. Publ. 26, 55– 79.

Huiqi, L., McClay, K.R., Powell, D., 1992. Physical models of thrust wedges. In: McCly K.R. (ed.) Thrust tectonics, 71-80.

Izquierdo-LlAvall, E., Aldega, L., Cantarelli, V., Corrado, S., Gil-Peña, I., Invernizzi, C., Casas-Sainz, A., 2013. On the origin of cleavage in the Central Pyrenees: Structural and paleo-thermal study. Tectonophysics, 608, 303–318.

Jagodzinski, H., 1949. Eindimensionale Fehlordnung in Kristallen und ihr Einfluss auf die Röntgen Interferenzen. Acta Crystallographica, 2, 201-207.

James, G.A., Wynd, J.G., 1965. Stratigraphic nomenclature of Iranian oil consortium agreement area. AAPG Bull., 49, 2182-2245.

Khadivi, S., Mouthereau, F., Larrasoaña, J-C., Vergés, J., Lacombe, O., Khademi, E., Beamud, E., Melinte-Dobrinescu, M., Suc, J-P., 2010 Magnetochronology of synorogenic Miocene foreland sediments in the Fars arc of the Zagros Folded Belt (SW Iran). Basin. Res., 22, 918-932. doi: 10.1111/j.1365-2117.2009.00446.x

Koop, W.J., Stoneley, R., 1982. Subsidence his- tory of the Middle East Zagros basin, Permian to recent. Philos. Trans. R. Soc. London, Ser. A, 305, 149-168.

Lacombe, O., Mouthereau, F., Kargar, S., Meyer, B., 2006. Late Cenozoic and modern stress fields in the western Fars (Iran): implications for the tectonic and kinematic evolution of Central Zagros. Tectonics, 25:TC1003, doi:10.1029/2005TC001831

Molinaro, M., Leturmy, P., Guezou, J-C., Frizon de Lamotte, D., 2005. The structure and kinematics of the south-eastern Zagros fold-thrust belt; Iran: from thin-skinned to thick-skinned tectonics. Tectonics, 24:TC3007. doi:10.1029/2004TC001633

Moore, D.M., Reynolds, R.C. Jr., 1997. X-Ray Diffraction and the identification and analysis of clay minerals. Oxford, UK, Oxford University Press, 378 pp.

Motamedi, H., Sherkati, S., Sepehr, M., 2012. Structural style variation and its impact on hydrocarbon traps in central Fars, Southern Zagros folded belt, Iran. J. Struct. Geol. 37, 124-133.

Mouthereau, F., Tensi, J., Bellahsen, N., Lacombe, O., Deboisgrollier, T., Kargar, S., 2007. Tertiary sequence of deformation in a thin-skinned/thick-skinned collision belt: the Zagros Folded Belt (Fars, Iran). Tectonics 26:TC5006. doi: 10.1029/2007TC002098

Mouthereau, F., Lacombe, O., Vergés, J., 2012. Building the Zagros collisional orogen: Timing, strain distribution and the dynamics of Arabia/Eurasia plate convergence. Tectonophysics 532–535:27-60. doi: 10.1016/j.tecto.2012.01.022

Najafi, M., Yassaghi, A., Bahroudi, A., Vergés, J., Sherkati, S., 2014. Impact of the Late Triassic Dashtak intermediate detachment horizon on anticline geometry in the Central Frontal Fars, SE Zagros Fold Belt, Iran. Mar. Pet. Geol. 54, 23-36.

Navabpour, P., Barrier, E., 2012. Stress states in the Zagros fold-and-thrust belt from passive margin to collisional tectonic setting. Tectonophysics, doi: 10.1016/j.tecto.2012.01.011

Navabpour, P., Angelier, J., Barrier, E., 2010. Mesozoic extensional brittle tectonics of the Arabian passive margin, inverted in the Zagros collision (Iran, interior Fars). Geological Society London Special Publications, 330, 65–96.

Pirouz, M., Simpson, G., Bahroudi, A., Azhdari, A., 2011. Neogene sediments and modern depositional environments of the Zagros foreland basin system. Geological Magazine 148 (5-6), 838-853.

Piryaei, A., Reijmer, J.J.G., Van Buchem, F.S.P., Yazdi-Moghadam, M., Sadouni J., Danelian, T., 2010. The influence of Late Cretaceous tectonic processes on sedimentation patterns along the northeastern Arabian plate margin (Fars Province, SW Iran), From: Leturmy, P. & Robin, C. (eds) Tectonic and Stratigraphic Evolution of Zagros and Makran during the Mesozoic–Cenozoic. Geological Society London Special Publications, 330, 211–251.

Pollastro, R.M., 1990. The illite/smectite geothermometer: concepts, methodology and application to basin history and hydrocarbon generation. In Nuccio, F., and Barker, C. E., eds. Application of thermal maturity studies to energy exploration. Denver, Rocky Mt. Sec., SEPM Spec. Publ., p. 1–18.

Powers, R.W. 1968. Saudi Arabia (excluding Arabian Shield). Centre National de la Recherche Scientifique, Lexique Stratigraphique International, III Asie, Fascicule 10b1.

Ruh, J.B., Hirt, A.M., Burg, J.-P., Mohammadi, A., 2014. Forward propagation of the Zagros Simply Folded Belt constrained from magnetostratigraphy of growth strata. Tectonics, 33, 1534–1551, doi:10.1002/2013TC003465.

Sclater, J.G., Christie, P.A.F., 1980. Continental stretching: An explanation of post–

Mid Cretaceous subsidence on the central North Sea Basin. Journal of Geophysical Research 85, 3711–3739.

Sepehr, M., Cosgrove, J.W., 2004. Structural framework of the Zagros Fold-Thrust Belt, Iran. Mar. Pet. Geol., 21, 829–843.

Sepehr, M., Cosgrove, J.W., 2005. Role of the Kazerun Fault Zone in the formation and deformation of the Zagros Fold-Thrust Belt, Iran. Tectonics 24:TC5005. doi:10.1029/2004TC001725

Setudehnia, A., 1972, Iran du Sud-Ouest: Lexiqu Strat. Internat., Centre Nat.Rech. Scientifique, Paris, III, Asie, Fasc.9b, 289-376.

Sherkati, S., Letouzey, J., 2004. Variation of structural style and basin evolution in the central Zagros (Izeh zone and Dezful embayment), Iran. Mar Pet Geol 21:535–554. doi: 10.1016/j.marpetgeo.2004.01.007

Sherkati, S., Molinaro, M., Frizon de Lamotte, D., Letouzey, J., 2005. Detachment folding in the Central and Eastern Zagros fold-belt (Iran): salt mobility, multiple detachments and late basement control. J Struct Geol 27:1680-1696. doi: 10.1016/j.jsg.2005.05.010

Sherkati, S., Letouzey, J., Frizon de Lamotte, D., 2006. Central Zagros fold-thrust belt (Iran): New insights from seismic data, field observation and sandbox modeling. Tectonics 25:TC4007. doi:10.1029/2004TC001766

Sweeney, J.J., Burnham, A.K., 1990. Evaluation of a simple model of vitrinite reflectance based on chemical kinetics. American Association of Petroleum Geologists Bulletin 74, 1559–1570.

Stocklin, J., 1968. Structural history and tectonics of Iran: A review. Am. Assoc. Pet. Geol. Bull., 52, 1223–1258.

Szabo, F., Kheradpir, A. 1978. Permian and Triassic stratigraphy, Zagros basin, southwest Iran. Journal of Petroleum Geology, 1, 57–82.

Talbot, C.J., Alavi, M., 1996. The past of a future syntaxis across the Zagros. In: Alsop GI, Blundell DJ, Davidson I (eds) Salt Tectonics. Geological Society London Special Publication 100, 89–109. doi: 10.1144/GSL.SP.1996.100.01.08

Vaziri-Moghaddam, H.,. Safari, I.A., Taheri, A., 2005. Microfacies, paleoenvironments and sequence stratigraphy of the Tarbur formation in kherameh area, SW Iran. Carbonates and Evaporites, 20, 131-137.

Vergés, J., Goodarzi, M.G.H., Emami, H., Karpuz, R., Efstathiou, J., Gillespie, P., 2011. Multiple Detachment Folding in Pusht-e Kuh Arc, Zagros: Role of Mechanical Stratigraphy. AAPG Mem. 94, 69-94.

Figure captions

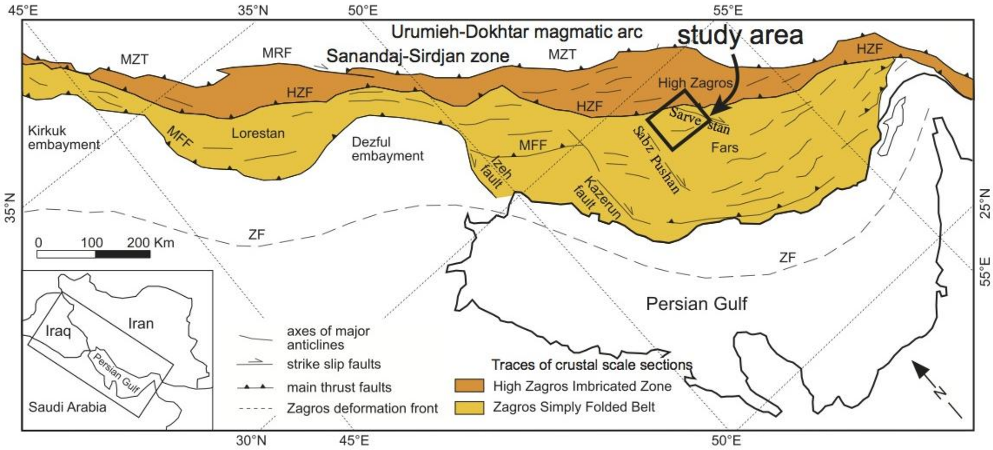

Figure 1: Structural map of the Zagros fold-and-thrust belt showing the major fault zones, the geological provinces and the study area in Fig. 2 (modified after Pirouz et al., 2011). HZF: High Zagros Fault, MFF: Zagros Mountain Frontal Fault, ZF: Zagros Front**.**

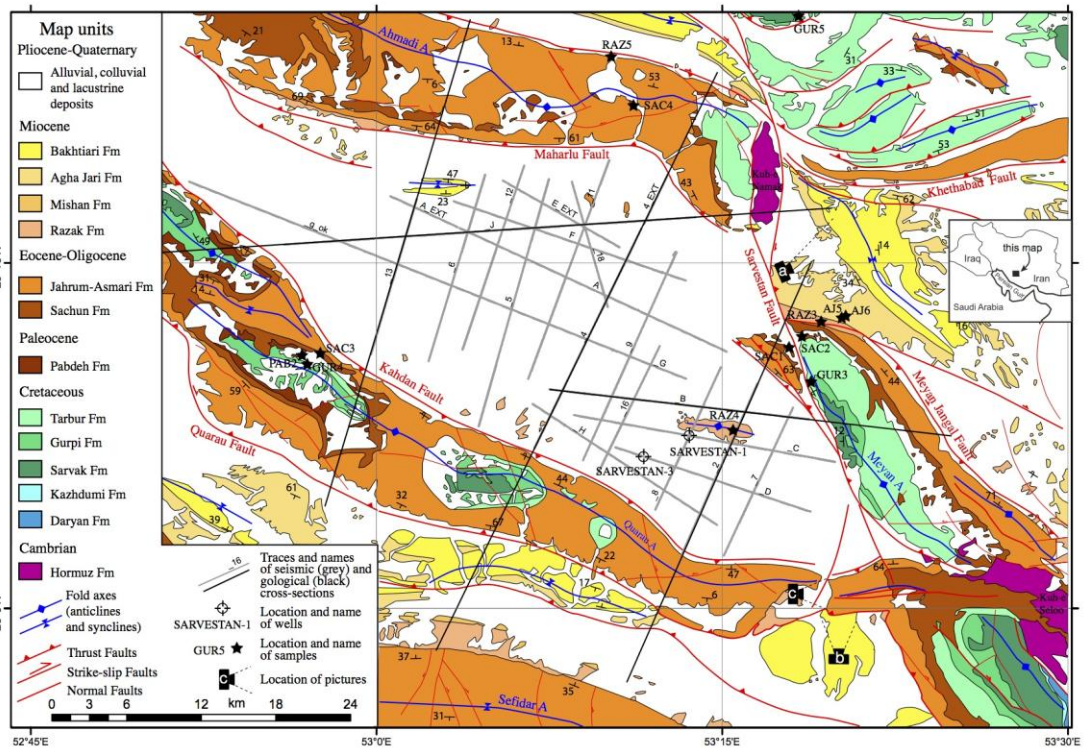

Figure 2: Geological map of the Sarvestan area (redrawn and modified from the following 1:100.000 sheets of the Geological Map of Iran: Kangan no. 20867W, Kushk no. 6647, and Sarvestan no. 6648). The location of interpreted seismic lines, of the Sarvestan-1 and Sarvestan-3 wells, the traces of the cross sections and the sampling sites are also shown.

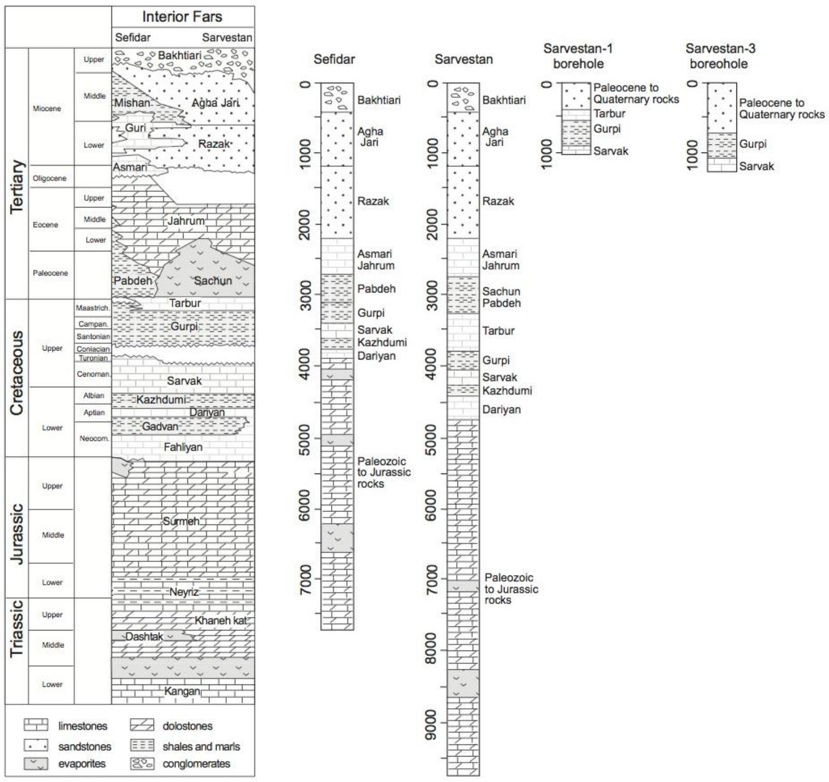

Figure 3: Stratigraphic correlation chart of the interior Fars (Sefidar and Sarvestan areas) Fars, showing lateral lithology and facies changes (modified after Sepehr and Cosgrove, 2004 for the Mesozoic-Cenozoic part). The stratigraphy of the Sarvestan-1 and Sarvestan-3 boreholes is also shown.

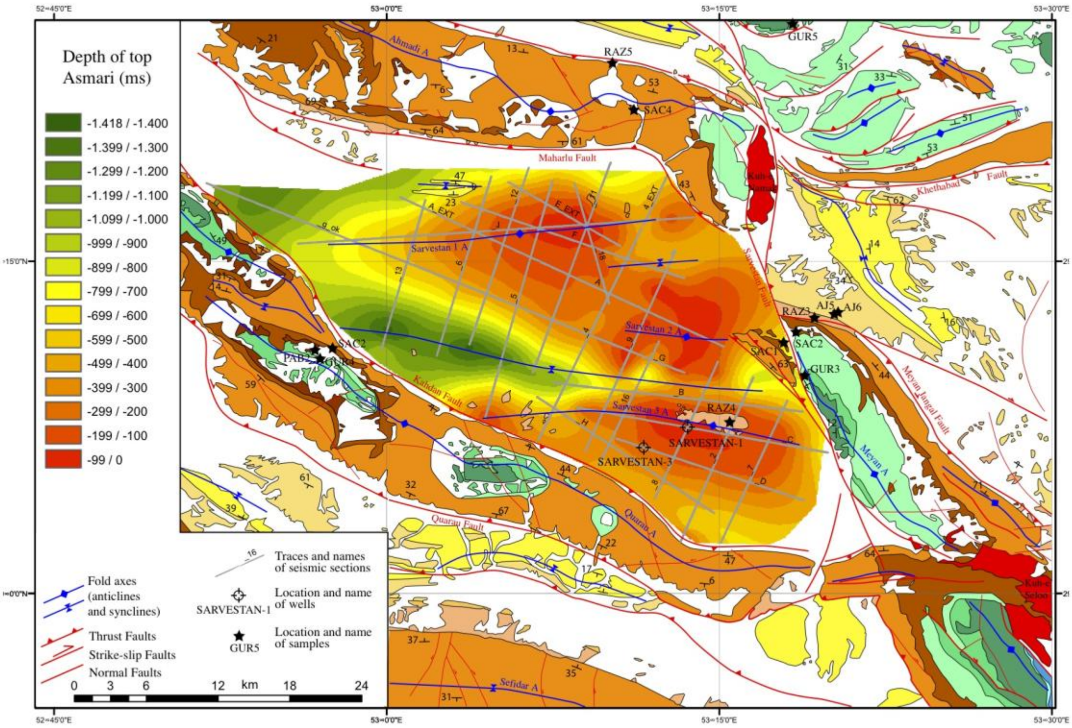

Figure 4: Structural map of the Top Asmari. The colours indicate the depth (TWT) of the top of the formation. The legend for the geological map is the same as in Fig. 2.

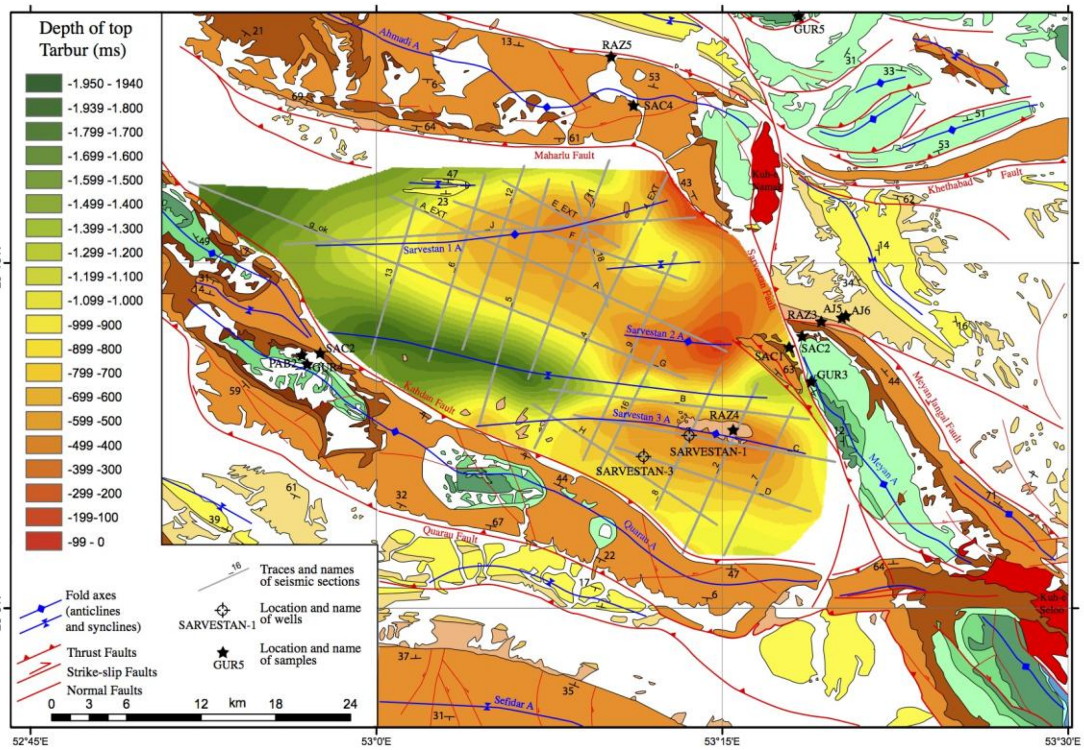

Figure 5: Structural map of the Top Tarbur. The colours indicate the depth (TWT) of the top of the formation. The legend for the geological map is the same as in Fig. 2.

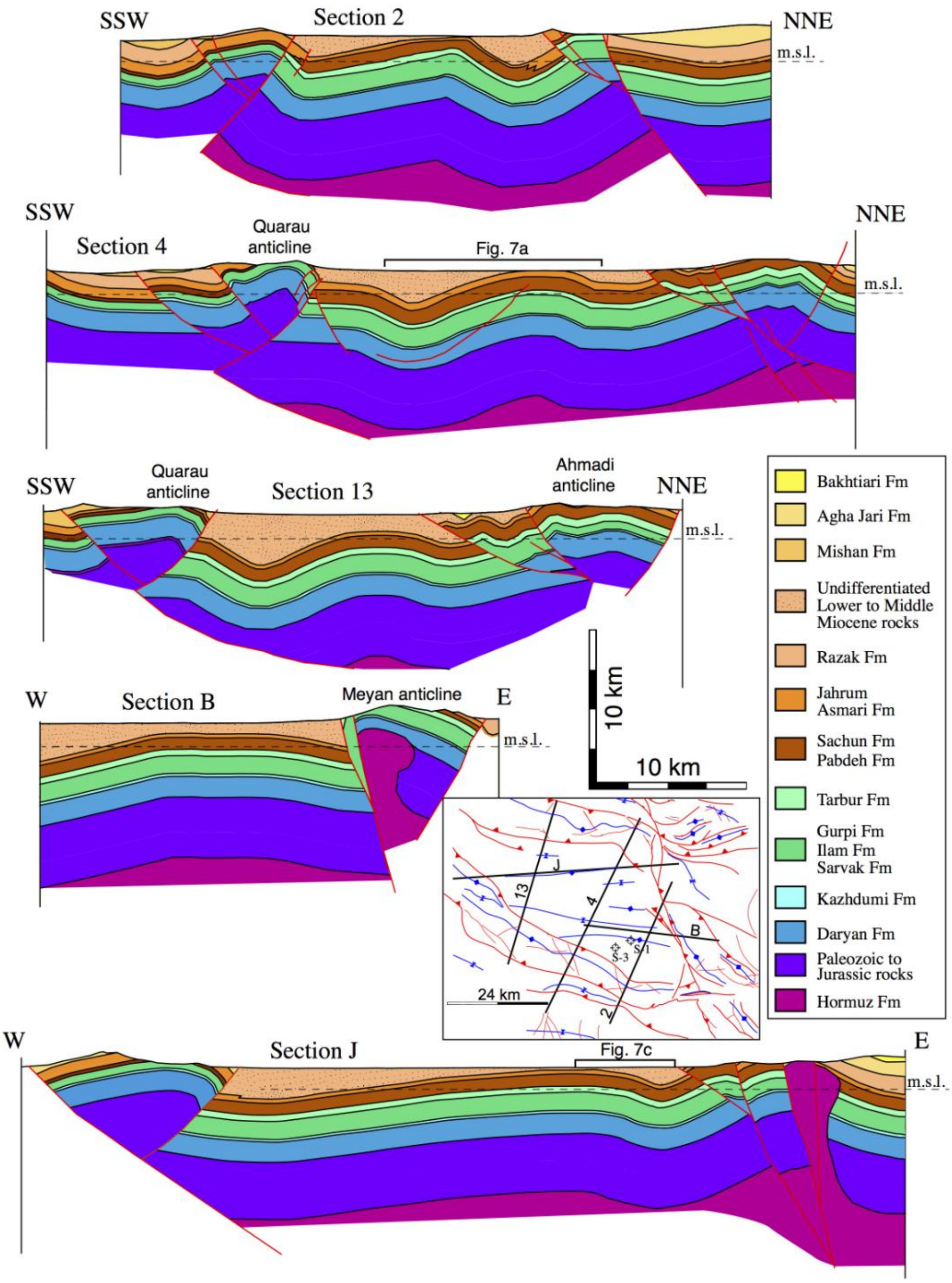

Figure 6: Geological cross sections across the Sarvestan area. Traces are shown in Fig. 2. Within the Sarvestan plain, the post-Asmari formations (Lower to Middle Miocene rocks) are undifferentiated, owing to the impossibility to distinguish them in seismic lines. The structural sketch showing the location of the geological cross-sections covers the same area of Fig. 2. The location of the correlation wells and of

the seismic sections drawn in Fig. 7 is also shown. S-1: Sarvestan-1 well; S-3: Sarvestan-3 well; m.s.l.: mean sea level.

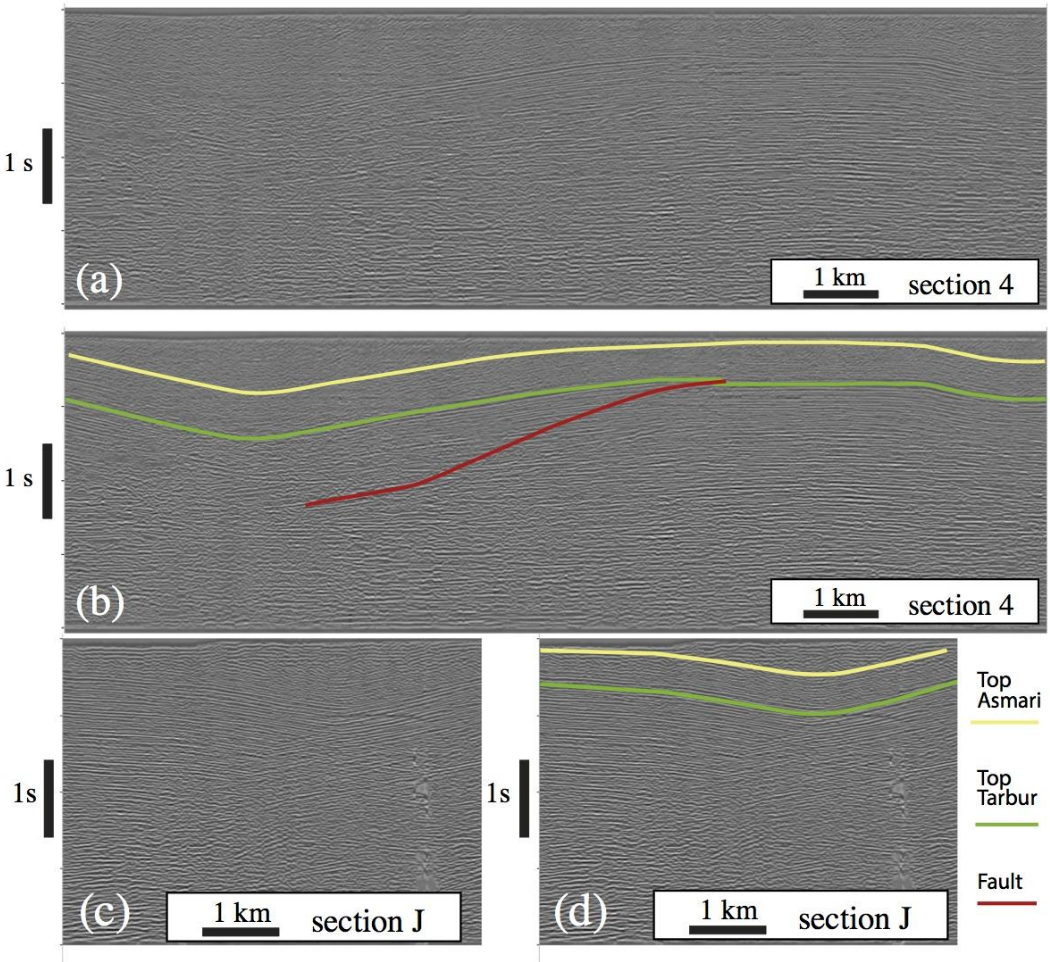

Figure 7: Seismic sections (and their interpretation) showing structures (folds and faults) buried beneath the Sarvestan plain. The position of the seismic sections is shown in Fig. 6.

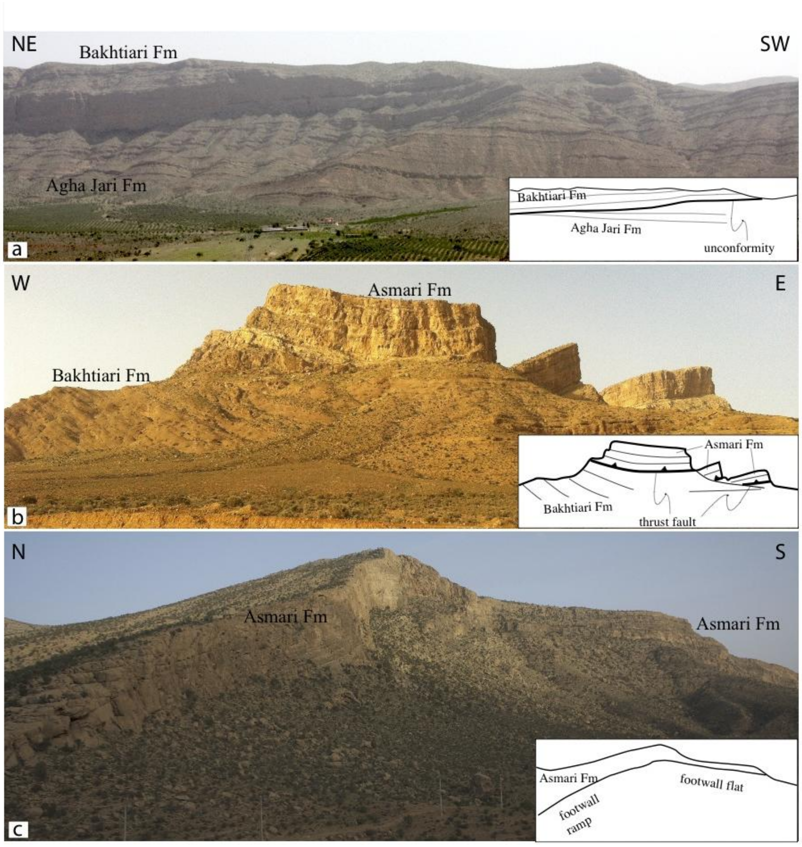

Figure 8: a) Angular unconformity between the Agha Jari and Bakhtiari Fms. b) Frontal view of the thrust fault bringing the Asmari Fm carbonates onto the Bakhtiari Fm conglomerates. c) Lateral view of the thrust fault of panel b. Notice the ramp-flat geometry of the Asmari Fm carbonates. The location of the pictures is shown in Fig. 2.

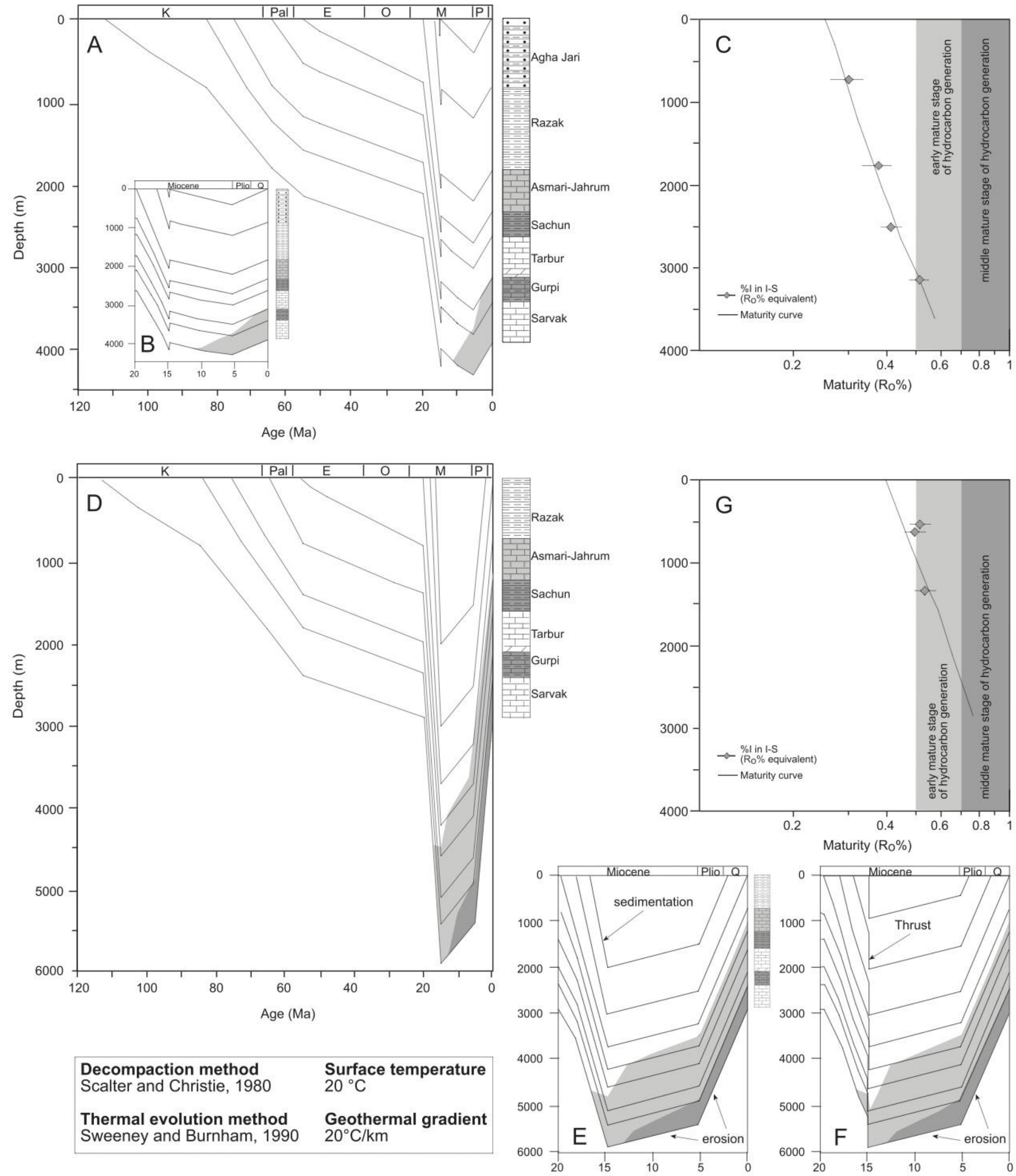

Figure 9: One-dimensional burial and thermal models of the Sarvestan fault hanging wall (A-C) and footwall (D-G): A) fault hanging wall in the last 120 Ma; B) fault hanging wall in the last 20 Ma; D) fault footwall in the last 120 Ma; E) thermal model of fault footwall in the last 20 Ma with sedimentation; F) thermal model of fault footwall in the last 20 Ma with thrust emplacement; C and G) Present-day maturity data plotted against calculated maturity curve.

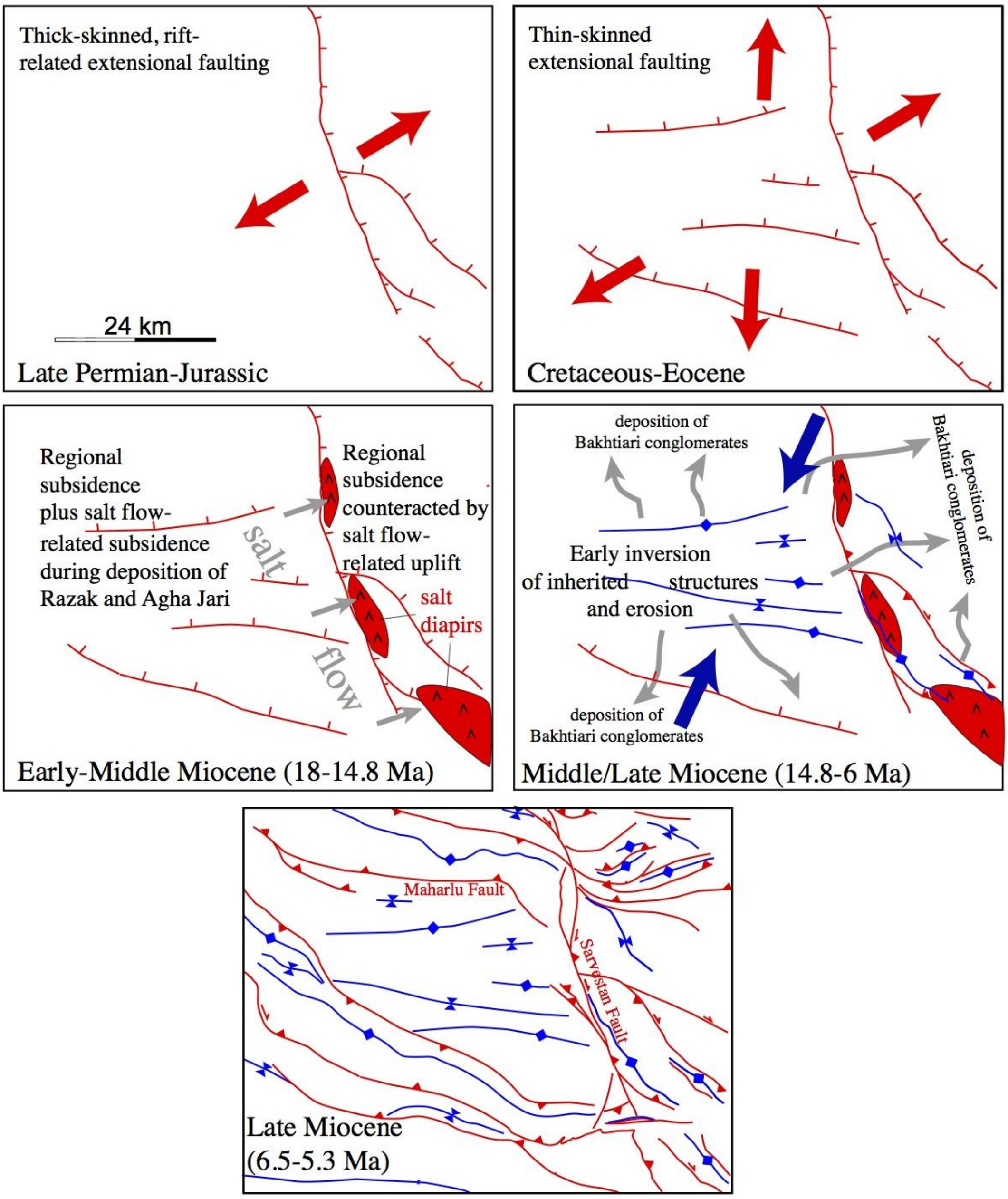

Figure 10: Evolutionary sketch for the Sarvestan area. The large arrows indicate extension (red) and shortening (blue) directions. The grey arrows indicate the paths of clastic sediments from source areas (characterized by early inversion of inherited structures) to depocenters. The scale is the same for all the panels. Structures are not palynspastically restored.

Tab. 1 - X-ray semi-quantitative analysis of the <2µm grain-size fraction. Pal=palygorskite; I= illite; I-S= mixed layer illite-smectite; C-S = mixed layer chlorite-smectite; K= kaolinite; Chl= chlorite; Qtz= quartz; Cal= calcite; Dol= dolomite; Ab= albite; Gy= gypsum; Go=goethite; R= stacking order (Jagodzinski, 1949); %I in I-S= illite content in mixed layer illite-smectite; %C in C-S= chlorite content in mixed layer chlorite-smectite.

Sample	Formation	Area	X-ray quantitative analysis of the <2µm grain-size fraction (%wt.)							R	%I in I-S	%C in C-S
			Pal	I	I-S	C-S	K	Chl	Other			
AJ6	Agha Jari		5	51	9	-	-	35	Qtz, Cal	0	30	-
RAZ3	Razak	Sarvestan	5	44	4	-	12	35	Qtz, Cal	0	40	-
SAC1	Sachun	Hanging wall	91	6	1	-	-	2	Dol, Ab, Gy	0	45	-
GUR3	Gurpi		-	20	24	43	7	6	Qtz, Cal	1	60	70
GUR5	Gurpi		-	49	11	-	40	-	Qtz, Cal	1	70	-
RAZ4	Razak		24	61	7	-	2	6	Qtz, Cal	1	70	-
RAZ5	Razak		-	42	22	-	32	4	Qtz, Cal	1	60	-
SAC2	Sachun	Sarvestan	93	2	5	-	-	-	Dol	1	65	-
SAC3	Sachun	Footwall	-	84	13	-	-	3	Dol, Go	1	74	-
PAB2	Pabdeh		-	34	53	-	6	7	Cal, Qtz	0	50	-
GUR4	Gurpi		-	27	37	-	36	-	Cal, Qtz	1	60	-

Table 1

Figure (with caption below and on the same page)
Click here to download high resolution image

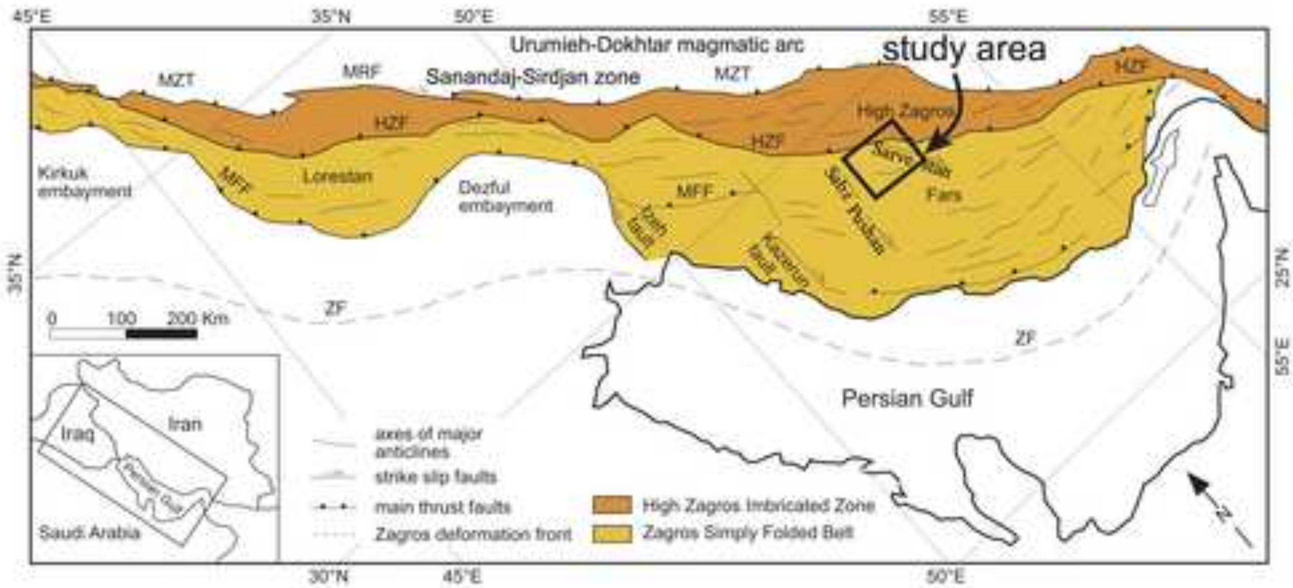

Figure (with caption below and on the same page)
Click here to download high resolution image

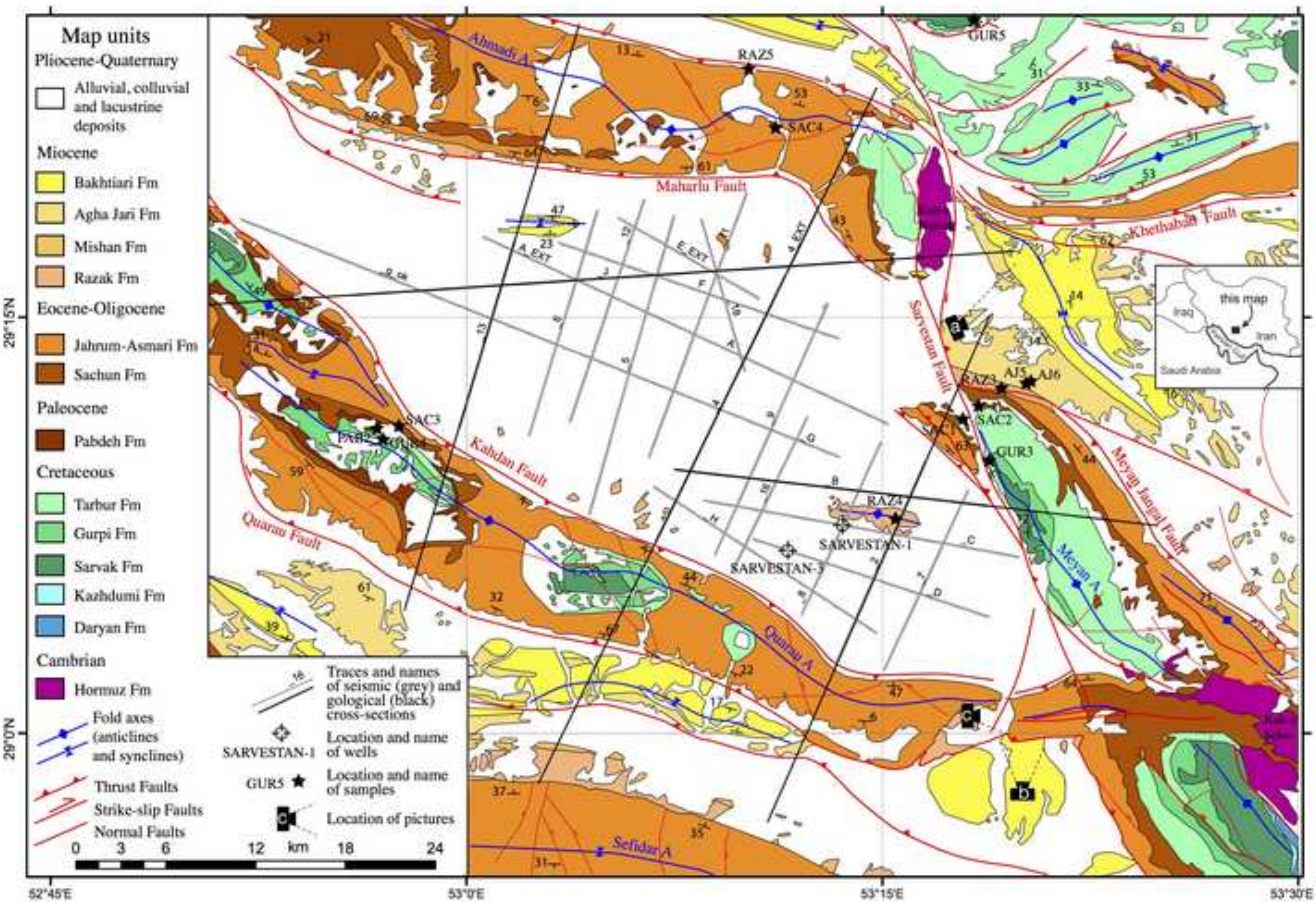

Figure (with caption below and on the same page)
Click here to download high resolution image

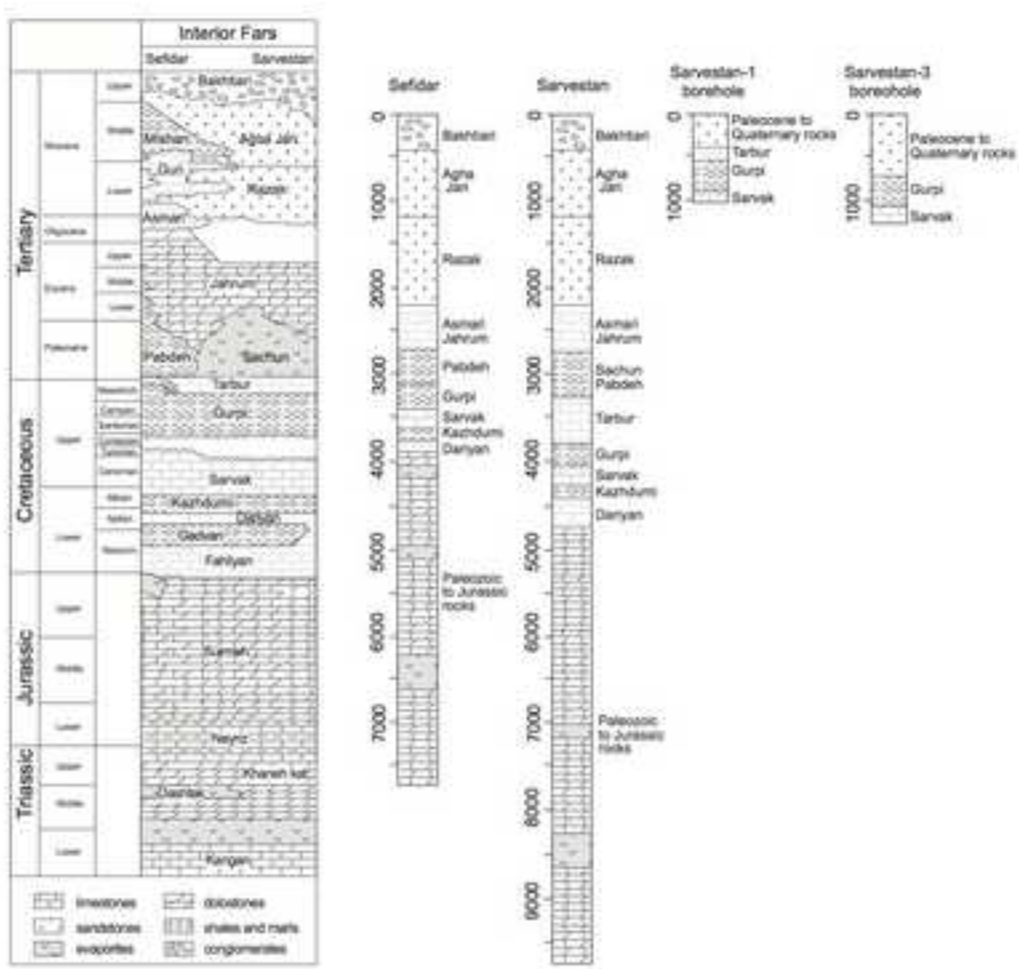

Figure (with caption below and on the same page)

Click here to download high resolution image

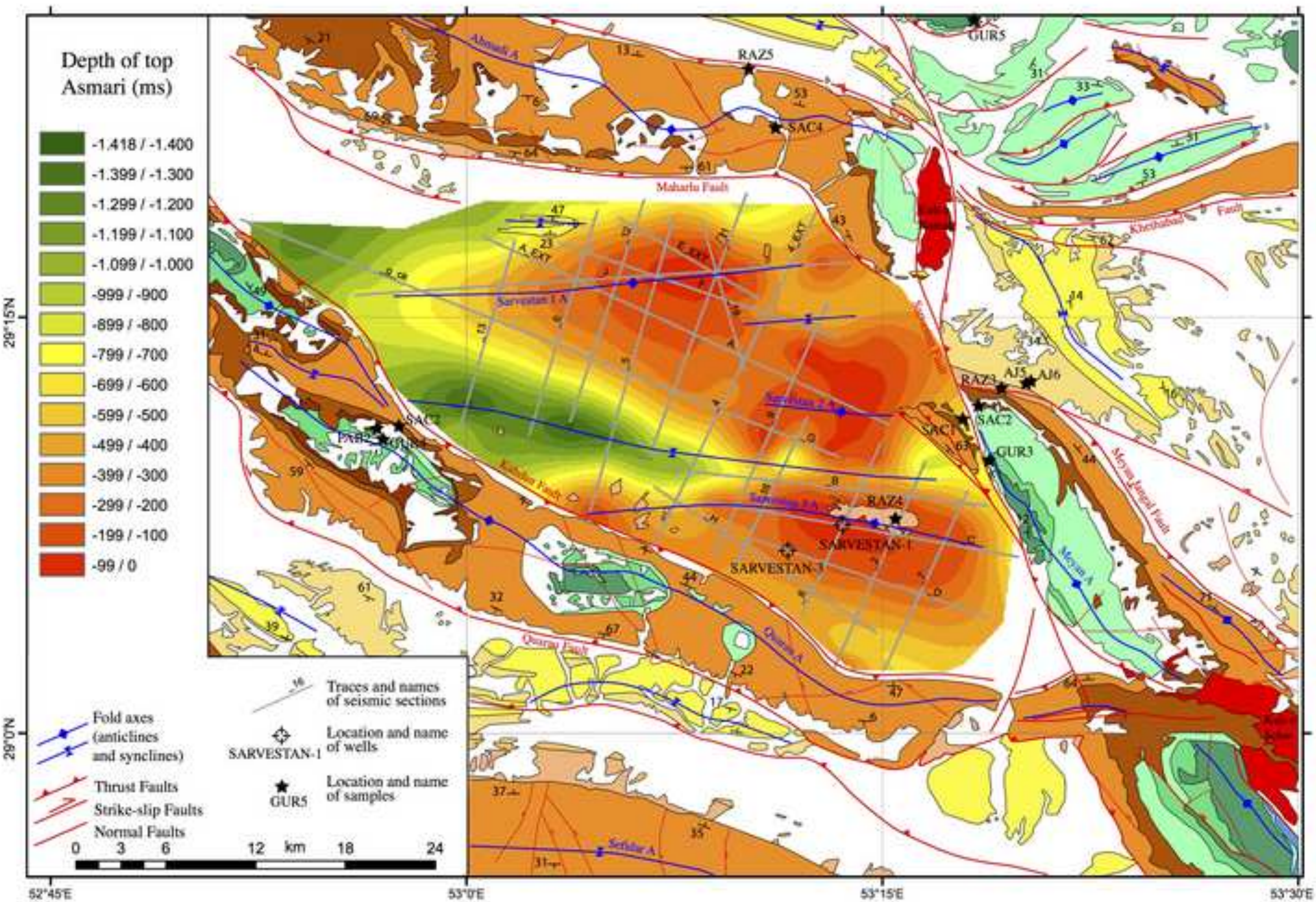

Figure (with caption below and on the same page)
Click here to download high resolution image

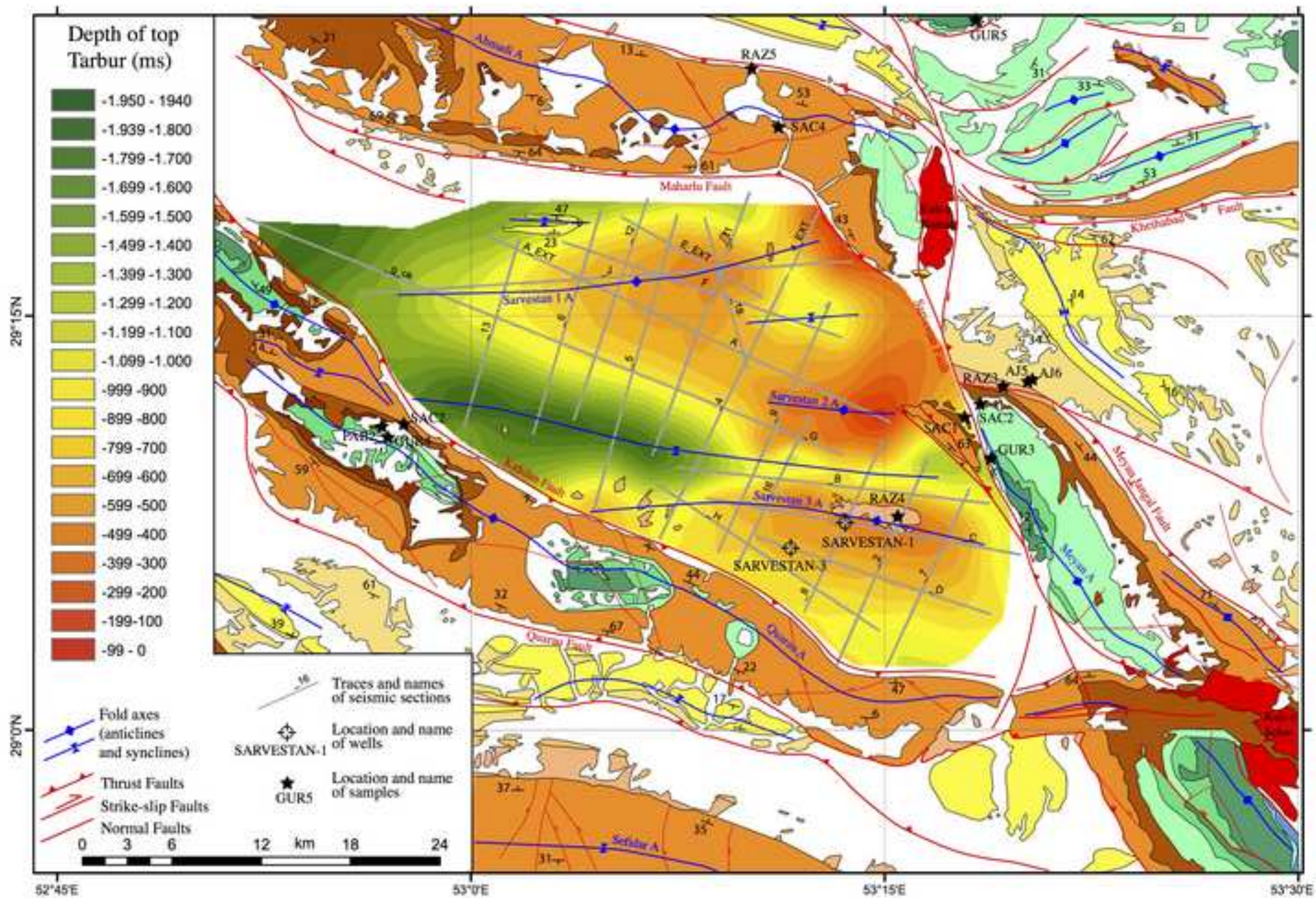

Figure (with caption below and on the same page)
Click here to download high resolution image

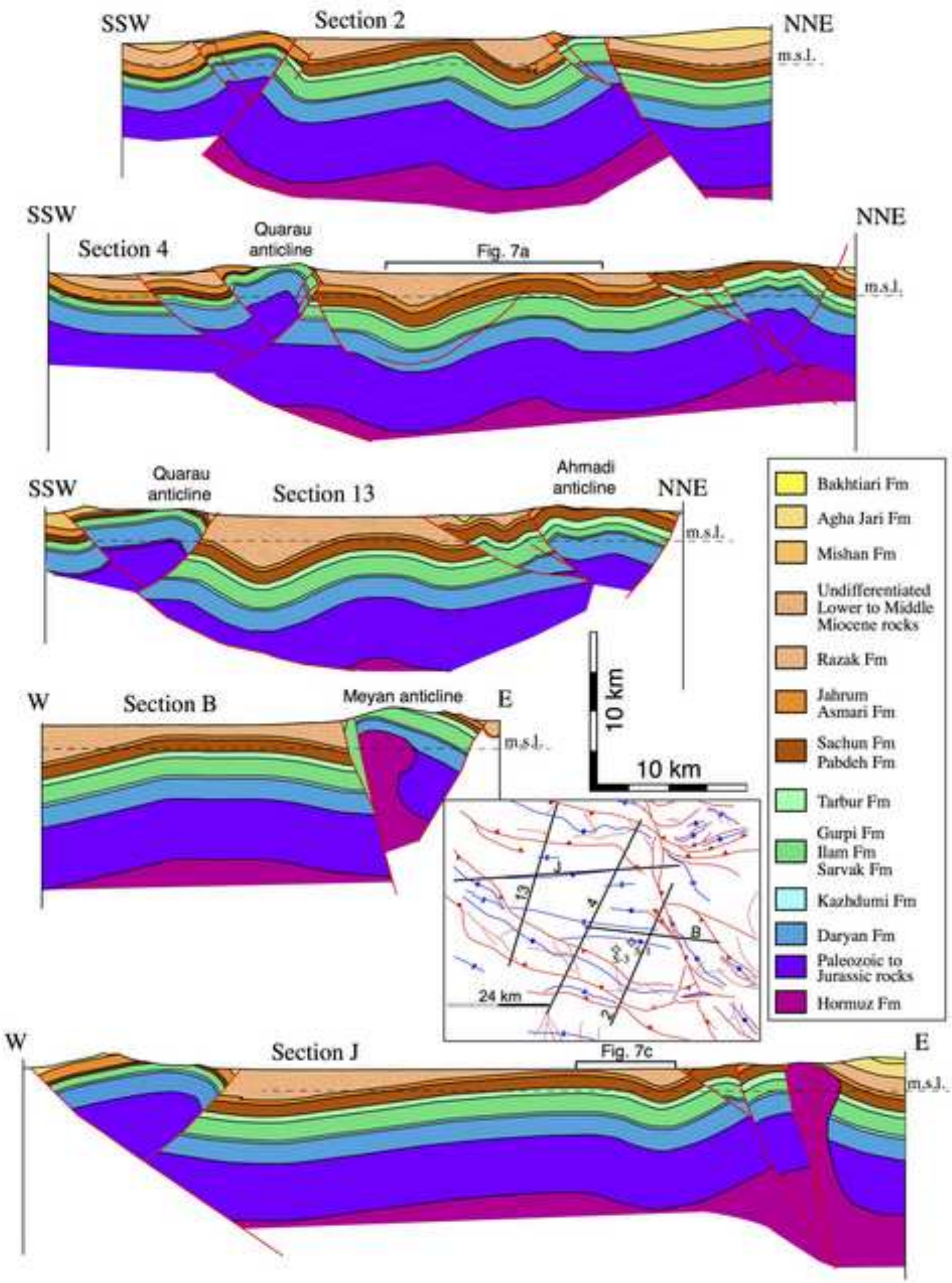

Figure (with caption below and on the same page)
Click here to download high resolution image

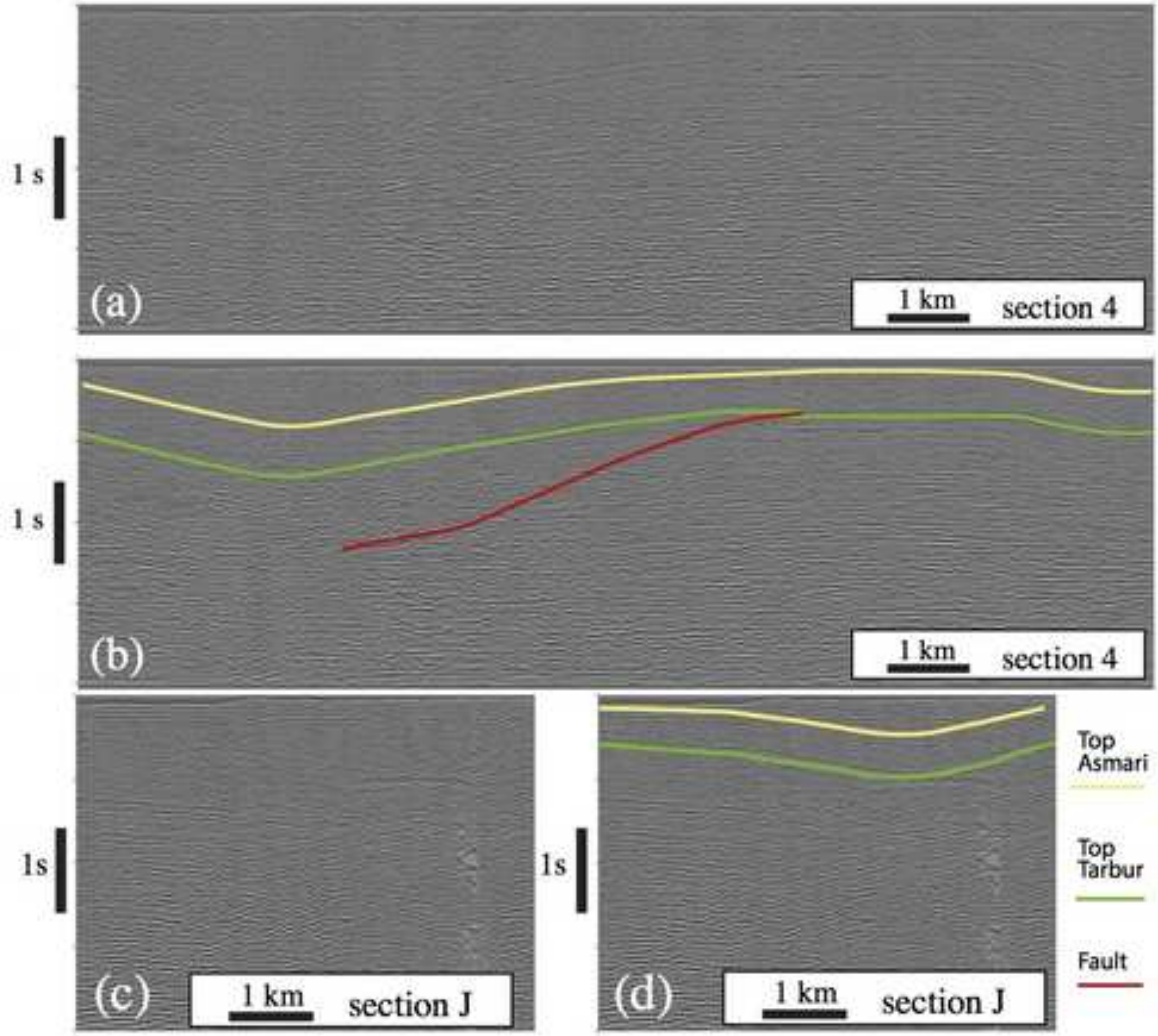

Figure (with caption below and on the same page)

Click here to download high resolution image

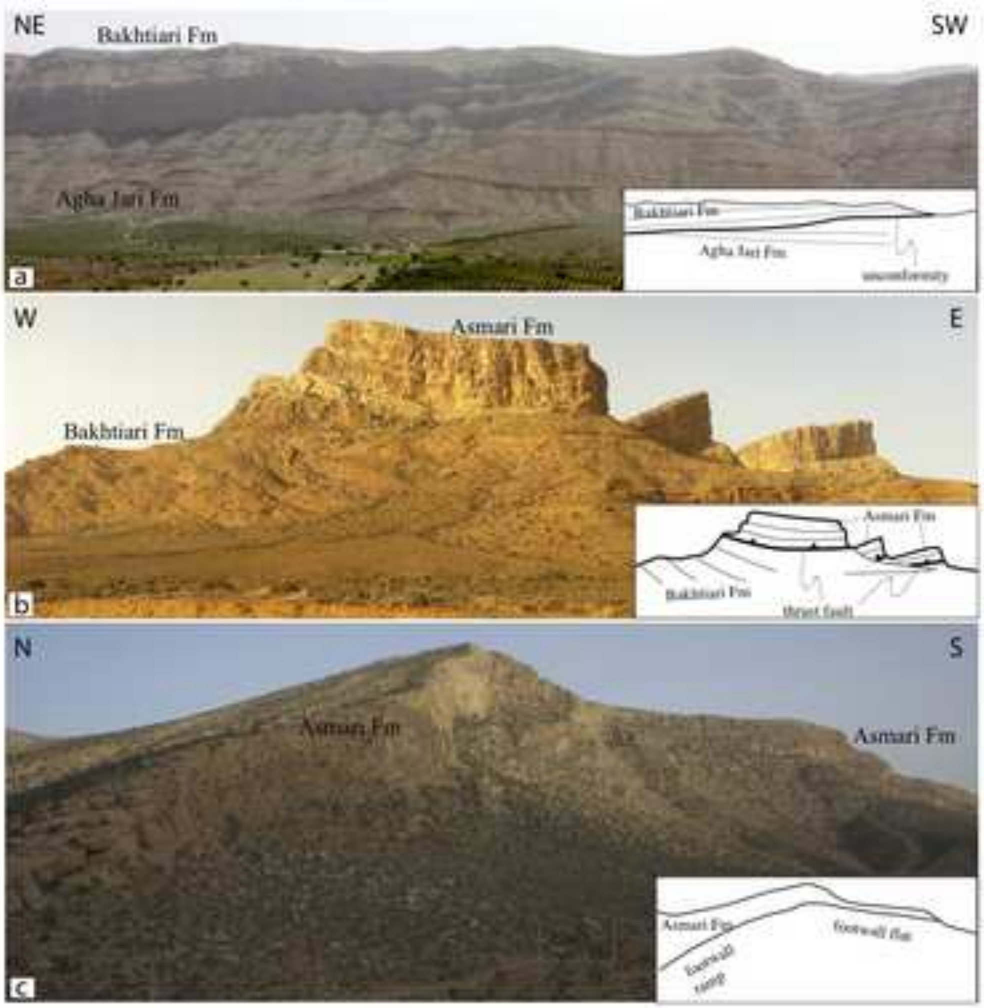

Figure (with caption below and on the same page)

Click here to download high resolution image

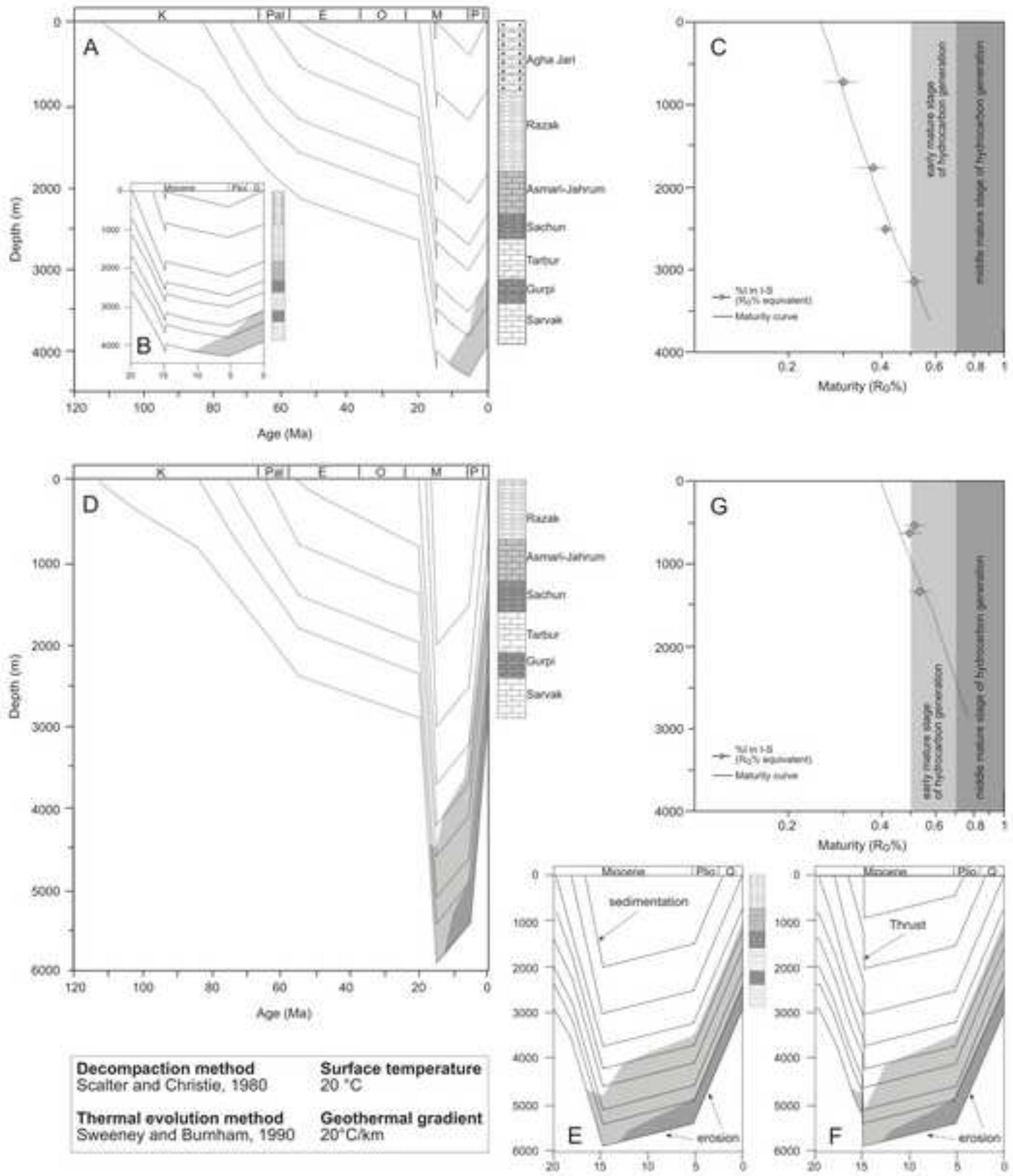

Figure (with caption below and on the same page)
Click here to download high resolution image